HHS Public Access

Author manuscript

Nat Methods. Author manuscript; available in PMC 2024 October 01.

Published in final edited form as:

Nat Methods. 2024 April ; 21(4): 692–702. doi:10.1038/s41592-024-02188-8.

Improved green and red GRAB sensors for monitoring spatiotemporal serotonin release *in vivo*

Fei Deng[1,2,3,8], **Jinxia Wan**[1,2,8], **Guochuan Li**[1,2], **Hui Dong**[1,2], **Xiju Xia**[1,2,4], **Yipan Wang**[1,2], **Xuelin Li**[1,2], **Chaowei Zhuang**[5], **Yu Zheng**[1,2,6], **Laixin Liu**[1,2,6], **Yuqi Yan**[1,2,6], **Jiesi Feng**[1,2], **Yulin Zhao**[1,2], **Hao Xie**[5], **Yulong Li**[1,2,4,6,7,*]

[1]State Key Laboratory of Membrane Biology, School of Life Sciences, Peking University, Beijing 100871, China.

[2]PKU-IDG/McGovern Institute for Brain Research, Beijing 100871, China.

[3]Institute of Molecular Physiology, Shenzhen Bay Laboratory, Shenzhen 518132, China.

[4]Peking University–Tsinghua University–National Institute of Biological Sciences Joint Graduate Program, Academy for Advanced Interdisciplinary Studies, Peking University, Beijing, China.

[5]Department of Automation, Tsinghua University, Beijing 100084, China.

[6]Peking-Tsinghua Center for Life Sciences, New Cornerstone Science Laboratory, Academy for Advanced Interdisciplinary Studies, Peking University, Beijing 100871, China.

[7]Chinese Institute for Brain Research, Beijing 102206, China.

[8]These authors contributed equally

Abstract

The serotonergic system plays important roles in both physiological and pathological processes, and is a therapeutic target for many psychiatric disorders. Although several genetically encoded GFP-based serotonin (5-HT) sensors were recently developed, their sensitivities and spectral profiles are relatively limited. To overcome these limitations, we optimized green fluorescent G-protein-coupled receptor (GPCR)-activation-based 5-HT ($GRAB_{5\text{-}HT}$) sensors and developed a red fluorescent $GRAB_{5\text{-}HT}$ sensor. These sensors exhibit excellent cell surface trafficking, high specificity, sensitivity, and spatiotemporal resolution, making them suitable for monitoring 5-HT dynamics *in vivo*. Besides recording subcortical 5-HT release in freely moving mice, we observed

*Manuscript correspondence: Yulong Li (yulongli@pku.edu.cn).

Author contributions

Y.L. conceived and supervised the project. F.D., G.L., J.W. and Yu Zheng developed and optimized the sensors. F.D., J.W. and G.L. performed the experiments related to characterizing the sensors with the help of X.X., Y.W., X.L. and Y.Y. J.W. performed the fiber photometry recordings with the help of H.D., L.L. and Yulin Zhao. F.D. performed the behavior assays, acute brain slice imaging and the mesoscopic imaging in head-fixed mice. H.X., F.D., C.Z. and J.F. built the mesoscopic imaging system. All authors contributed to the data interpretation and analysis. F.D. and Y.L. wrote the manuscript with input from all other authors, especially the review and editing from Yulin Zhao.

Competing interests

The authors declare no competing interests.

Code availability

The custom-written MATLAB, Arduino, and ImageJ programs are available under an MIT license from https://github.com/yulonglilab.

both uniform and gradient 5-HT release in the mouse dorsal cortex with mesoscopic imaging. Finally, we performed dual-color imaging and observed seizure-induced waves of 5-HT release throughout the cortex following calcium and endocannabinoid waves. In summary, these 5-HT sensors can offer valuable insights regarding the serotonergic system in both health and disease.

Introduction

Serotonin (5-HT) is an important monoamine signaling molecule present virtually throughout the body, regulating a wealth of biological processes[1]. In the central nervous system (CNS), 5-HT is an intensively studied neuromodulator involved in a wide range of neurobiological processes such as emotion, learning and memory, reward, appetite, and sleep-wake cycles[1–3]. Moreover, impaired 5-HT transmission is associated with a broad range of CNS disorders, including anxiety, addiction, depression, and epilepsy[4–6]. As a consequence, many psychotropic and psychedelic drugs have been developed to target the serotonergic system[7]. Therefore, understanding the serotonergic transmission in both physiological and pathological processes requires the ability to directly monitor 5-HT dynamics in behaving animals in real time, which requires sensitive detection tools. Although classic detection methods such as microdialysis and fast-scan cyclic voltammetry provide valuable accesses for measuring 5-HT levels, they lack the simultaneous high spatiotemporal resolution, specificity, sensitivity, and minimal invasiveness needed for the *in vivo* detection of 5-HT[8–10].

Recent advances in genetically encoded fluorescent 5-HT sensors have led to tools that surpass classic methods; however, these sensors have not yet hit the proverbial “sweet spot” with respect to balancing apparent affinity with the magnitude of the response. Specifically, sensors based on GPCRs, including $GRAB_{5\text{-}HT1.0}$, PsychLight2 and sDarken[11–13], have high affinity for 5-HT but produce only a modest change in fluorescence. The periplasmic binding protein based sensor iSeroSnFR[14] has a large response, but low affinity to 5-HT. Thus, monitoring 5-HT dynamics *in vivo* requires a more sensitive sensor, with a high affinity and sufficiently large response.

In the CNS, the serotonergic system interacts with other neurotransmitters and neuromodulators[15]; thus, simultaneously imaging 5-HT and other neurochemicals can provide valuable information regarding the regulation of cognitive functions controlled by these signaling processes. Unfortunately, most existing sensors for neurochemicals contain a green fluorescent protein (GFP) as the fluorescent module, as do all genetically encoded 5-HT sensors, precluding combined imaging due to spectral overlap. Although a near-infrared 5-HT nanosensor based on single-wall carbon nanotubes has been reported[16], it may not be suitable for use in living animals due to limited sensitivity. On the other hand, red-shifted sensors, such as a previously reported red calcium sensor[17], are compatible with other green fluorescent sensors and blue light-excitable actuators, with intrinsically superior optical properties—including deeper tissue penetration, reduced autofluorescence, and low phototoxicity—due to their longer excitation wavelengths. Thus, red-shifted 5-HT sensors suitable for *in vivo* imaging, particularly multiplexed imaging, are needed.

Here, we report a series of green and red fluorescent 5-HT sensors based on the 5-HTR4 subtype. The green fluorescent sensor, $gGRAB_{5\text{-}HT3.0}$ (g5-HT3.0), produces a ~1,300% fluorescence increase to 5-HT, making it superior to existing green fluorescent 5-HT sensors both *in vitro* and *in vivo*. The red-shifted sensor, $rGRAB_{5\text{-}HT1.0}$ (r5-HT1.0), produces a >300% fluorescence increase to 5-HT *in vitro* and is suitable for multicolor imaging *in vivo*. Moreover, using mesoscopic imaging, we have revealed distinct 5-HT releasing patterns under different conditions.

Results

Development and optimization of $GRAB_{5\text{-}HT}$ sensors

To expand the dynamic range and spectral profile of $GRAB_{5\text{-}HT}$ sensors, we first systematically searched for the most suitable GPCR scaffold by transplanting the ICL3 from existing green and red fluorescent GRAB sensors into a wide range of 5-HT receptor subtypes (Fig. 1a). For green fluorescent sensors, we used green $GRAB_{5\text{-}HT1.0}$ (g5-HT1.0) or $GRAB_{NE1m}$[18] derived ICL3 as the donor (including cpEGFP and surrounding linkers). Possibly due to the conserved structures among the class A family of GPCRs, we obtained candidate sensors that yielded a >50% increase in fluorescence ($\Delta F/F_0$) in response to 10 μM 5-HT following the screening of replacement sites. One green fluorescent candidate based on 5-HTR4 had a higher response than the original g5-HT1.0 sensor and was named g5-HT1.1. To develop red fluorescent 5-HT sensors, we transplanted the ICL3 derived from $rGRAB_{DA1m}$[19] into the 5-HTR2C, 5-HTR4, and 5-HTR6 scaffolds—we chose these three subtypes based on their high performance when developing the green fluorescent 5-HT sensors. The top candidate was still based on the 5-HTR4 subtype, with a ~40% $\Delta F/F_0$; we named it r5-HT0.1 (Fig. 1a).

To improve the sensors' sensitivity, then we optimized g5-HT1.1 and r5-HT0.1 by performing saturation mutagenesis of critical residues believed to affect structural coupling, fluorescence intensity[20], protein folding[21], and conformational change[22].

Further iterative optimization by screening more than 4,500 candidates yielded two intermediate green fluorescent sensors called g5-HT2h and g5-HT2m, followed by the final sensor g5-HT3.0 (Fig. 1b,c and Supplementary Fig. 1a–c). When expressed in HEK293T cells, these green fluorescent 5-HT sensors showed good trafficking to the cell surface and a robust fluorescence increase to 100 μM 5-HT application (Fig. 1c,d and Extended Data Fig. 1a–c). Importantly, g5-HT3.0 ($\Delta F/F_0$: ~1,300%) showed much larger response than g5-HT1.0, PsychLight2, and iSeroSnFR. Moreover, g5-HT3.0 is much brighter, with a higher signal-to-noise ratio (SNR) than other 5-HT sensors (Fig. 1d). Dose-response curves showed that g5-HT3.0 produces a larger $\Delta F/F_0$ than previous sensors over a wide range of concentrations, with an EC_{50} value of ~150 nM (Fig. 1e). We also generated a 5-HT insensitive version of g5-HT3.0, named g5-HT3.0mut, by introducing the $p.D131^{3.32}F$ (superscript 3.32 defined by the Ballesteros–Weinstein numbering system) substitution[22, 23]; we confirmed that g5-HT3.0mut localizes to the plasma membrane but does not respond to 5-HT even at 100 μM (Fig. 1b–e and Supplementary Fig. 1a,c).

Similarly, we generated a red fluorescent 5-HT sensor called r5-HT1.0 by screening >3,000 candidates, and a 5-HT insensitive version, named r5-HTmut, by introducing the p.D131$^{3.32}$Q and p.D149$^{3.50}$H mutations (Fig. 1b–e and Supplementary Fig. 1d,f). Both r5-HT1.0 and r5-HTmut localized to the plasma membrane when expressed in cultured HEK293T cells (Fig. 1c). Application of 10 μM 5-HT to cells expressing r5-HT1.0 elicited a ~330% fluorescence increase, but had no effect on cells expressing r5-HTmut (Fig. 1c,d). The EC_{50} of r5-HT1.0 was ~790 nM (Fig. 1e). Moreover, unlike the cpmApple-based calcium sensor jRGECO1a—in which blue light causes an increase in fluorescence[17]—r5-HT1.0 did not show obvious photoactivation as jRGRECO1a (Fig. 1f), suggesting its compatibility with blue-light-excitable optogenetic opsins or green fluorescent sensors, despite that it exhibited a small off response when exposed to intense blue-light illumination up to 10 mW (Extended Data Fig. 1k,l).

Characterization of $GRAB_{5\text{-}HT}$ sensors

Next, we characterized the pharmacology, specificity, spectra, and kinetics of these 5-HT sensors expressed in HEK293T cells. We found that both g5-HT3.0 and r5-HT1.0 inherited the pharmacological specificity of the parent 5-HTR4 receptor, as their 5-HT induced responses were blocked by the 5-HTR4-specific antagonist RS 23597-190 (RS), but not the 5-HTR2C-specific antagonist SB 242084 (SB); in addition, both sensors were unaffected by application of a wide range of signaling molecules, including the 5-HT precursor, 5-HT metabolite, and a variety of other neurotransmitters and neuromodulators (Fig. 2a and Extended Data Fig. 2a,b). The emission spectra of the green fluorescent (with a peak at 520 nm) and red fluorescent (with a peak at 595 nm) sensors are well-separated, and 1-photon/2-photon excitation peaks for g5-HT3.0 and r5-HT1.0 are at 505/920 nm and 560/1050 nm, respectively (Fig. 2b and Extended Data Fig. 1d,e). The isosbestic point for g5-HT3.0 under 1-photon excitation is 425-nm. Regarding the sensors' kinetics, we measured the on rate (τ_{on}) by locally puffing 10 μM 5-HT on the cells and the off rate (τ_{off}) by puffing the 5-HTR4 antagonist RS in the continued presence of 10 μM 5-HT (Fig. 2c,d), revealing sub-second τ_{on} rates and faster τ_{off} rates than our previously reported g5-HT1.0 sensor[11], with mean τ_{off} rates of 1.66 s, 1.90 s, 0.38 s, and 0.51 s for g5-HT3.0, g5-HT2h, g5-HT2m, and r5-HT1.0, respectively (Fig. 2e and Extended Data Fig. 1f).

We then expressed the g5-HT3.0 and r5-HT1.0 sensors in cultured rat cortical neurons and found that they trafficked well to the cell membrane. Application of a saturating concentration of 5-HT induced a fluorescence increase of ~2,700% for g5-HT3.0 and ~400% for r5-HT1.0, but had no effect on neurons expressing g5-HT3.0mut or r5-HTmut (Fig. 2f,g,i,j). In cultured cortical neurons, EC_{50} values of g5-HT3.0, g5-HT2h, g5-HT2m, and r5-HT1.0 were 80 nM, 70 nM, 2.4 μM, and 600 nM, respectively (Fig. 2h,k and Extended Data Fig. 1g), and they exhibited high specificity to 5-HT (Extended Data Fig. 2c–f). Compared to previously reported GFP-based 5-HT sensors, g5-HT3.0 showed larger brightness, a greater fluorescence change, and higher SNR in cultured neurons (Extended Data Fig. 3).

To investigate whether our 5-HT sensors couple to downstream signaling pathways, we employed the luciferase complementation assay[24] and the Tango assay[25] to measure the

GPCR-mediated G_s and β-arrestin pathways, respectively. These sensors showed negligible downstream coupling; in contrast, the wild-type 5-HTR4 receptor had high basal activity and robust, dose-dependent coupling (Fig. 2l and Extended Data Fig. 1h,i). In addition, our sensors do not undergo β-arrestin-mediated internalization or desensitization when expressed in cultured neurons, as the 5-HT elicited increase in fluorescence was stable for up to 2 hours in the continuous presence of 10 μM 5-HT (Fig. 2m and Extended Data Fig. 1j). Furthermore, expression of these sensors showed minimal buffering effects *in vitro* and did not have obvious impact on 5-HT-related behaviors (Extended Data Fig. 4). This suggests that these sensors are well-suited for monitoring serotonin dynamics without affecting normal cell physiology and animal behaviors.

Using the sensitive g5-HT3.0 sensor and a red dopamine (DA) sensor, $rGRAB_{DA3m}$ (rDA3m)[26], we performed dual-color confocal imaging in the mouse dorsal raphe nucleus (DRN) to simultaneously monitor the 5-HT and DA dynamics with high spatial-temporal resolution. Unlike the synchronous releases elicited by electrical stimulation, the spontaneous transients are separated, with a higher frequency of 5-HT events compared to those of DA (Extended Data Fig. 5). Importantly, g5-HT3.0 demonstrated remarkable sensitivity in detecting spontaneous release events with a diameter as small as ~10 μm, suggesting its potential to detect single-cellular or even sub-cellular 5-HT release in micron-scale.

Measuring endogenous 5-HT release in freely moving mice

To determine whether our red fluorescent sensor is capable of monitoring endogenous 5-HT dynamics *in vivo*, we expressed either r5-HT1.0 or r5-HTmut in the basal forebrain (BF) and channelrhodopsin-2 (ChR2)[27] in serotonergic neurons in the DRN of *Sert-Cre* mice[28] (Fig. 3a). Optical stimulation of the DRN induced time-locked transient increases in r5-HT1.0 fluorescence, the amplitude of which increased progressively with increasing stimulation duration; moreover, the selective serotonin transporter (SERT) inhibitor fluoxetine further increased the response amplitude and prolonged the response's decay time (Fig. 3b–e). As expected, no response was measured for the 5-HT insensitive r5-HTmut sensor (Fig. 3b–e).

To leverage the red-shifted 5-HT sensor's spectrum with green fluorescent sensors, we expressed either r5-HT1.0 or r5-HTmut in the BF and expressed the axon-targeted green fluorescent calcium sensor axon-GCaMP6s[29] in DRN serotonergic neurons of *Sert-Cre* mice, which project to the BF and regulate sleep-wake cycles[11, 30]. We then performed dual-color fiber photometry recording in the BF while simultaneously recording the electroencephalography (EEG) and electromyography (EMG) signals to track the animal's sleep-wake state (Fig. 3f). We found that both the r5-HT1.0 and GCaMP6s signals were higher during the wake state and NREM (non-rapid eye movement) sleep than during REM sleep (Fig. 3g,j). Additionally, r5-HT1.0 revealed oscillations in 5-HT levels (Fig. 3h). Moreover, the r5-HT1.0 and GCaMP6s signals were temporally correlated, with no detectable lag, revealing the rapid release of 5-HT and high consistency between 5-HT release and the increase in presynaptic calcium (Fig. 3i). In contrast, the r5-HTmut signal was largely unchanged throughout sleep-wake cycles (Fig. 3j and Extended Data Fig. 6).

To compare the performance of our optimized g5-HT3.0 sensor to previously reported 5-HT sensors, we also performed bilateral recordings in the BF during sleep-wake cycles in mice expressing g5-HT3.0 in one hemisphere and g5-HT1.0, PsychLight2, or iSeroSnFR in the other hemisphere (Extended Data Fig. 7a,d,g). We found that the g5-HT3.0 sensor had larger SNR during the wake state and NREM sleep compared to the other three sensors, as well as more robust oscillations measured during NREM sleep (Extended Data Fig. 7b,c,e,f,h,i). Moreover, g5-HT3.0 exhibited greater sensitivity compared to g5-HT1.0 and iSeroSnFR in detecting modest 5-HT changes, such as in the basal amygdala (BA) of the water-restricted mice during 5% glucose delivery (Extended Data Fig. 8).

Additionally, we observed that sensors in mice injected with higher-titer virus exhibited a larger SNR than those injected with lower-titer virus during sleep-wake cycles in the BF, underscoring the importance of selecting an appropriate virus titer (Supplementary Fig. 2).

Mesoscopic imaging of cortical 5-HT dynamics in mice

While 5-HT plays crucial roles in the cerebral cortex, its serotonergic projections are notably sparser compared to subcortical regions like the BF[31]. Therefore, measuring 5-HT release in the cortex requires a highly sensitive 5-HT sensor. We expressed the g5-HT3.0 sensor in neurons throughout the whole brain by injecting AAVs into the transverse sinus of neonatal (postnatal day, P0–P1) mice[32]. We then measured g5-HT3.0 fluorescence throughout the whole dorsal cortex using mesoscopic imaging[33] in response to optogenetic stimulation of DRN serotonergic neurons expressing ChrimsonR[34] (Fig. 4a). We found that light pulses induced transient increases in g5-HT3.0 fluorescence, with increasing stimulation frequency causing increasingly larger responses (Fig. 4b,c). As a negative control, no response was measured when we expressed a membrane-tethered EGFP (memEGFP) (Fig. 4 b,c and Extended Data Fig. 9g). Importantly, we found that treating mice with SERT blocker fluoxetine caused a gradual increase in baseline 5-HT levels and slowed the decay rate of stimulation-induced transients; in contrast, the dopamine transporter (DAT) blocker GBR 12909 had no effect (Fig. 4d and Extended Data Fig. 9a–f).

We then used g5-HT3.0 to measure physiological 5-HT dynamics during sleep-wake cycles using mesoscopic imaging combined with simultaneous EEG and EMG recordings. Similar to our results measured in the subcortical BF (Extended Data Fig. 7), the g5-HT3.0 signal in the dorsal cortex was highest during the wake state, followed by the NREM and REM states, with oscillations during NREM sleep. Moreover, we found no change in fluorescence through sleep-wake cycles using g5-HT3.0mut (Fig. 4e,f).

We further segmented the dorsal cortex into various brain regions based on the Allen Common Coordinate Framework v3 (CCFv3) atlas[35] and analyzed the spatial distribution of the 5-HT signals during optogenetic stimulation and sleep-wake cycles. We found that the 5-HT signals measured in different brain regions were relatively spatially homogenous and temporally synchronized during sleep-wake cycles (Fig. 4g and Extended Data Fig. 9h), reminiscent of our previous results recorded in subcortical regions[11]. In contrast, when we optogenetically stimulated DRN serotonergic neurons, the 5-HT signals had a graded pattern, decreasing along the anterior-to-posterior axis (Fig. 4g,h); this pattern

was consistent with the anatomically heterogeneous density of serotonergic projections throughout the cortex[31].

These results demonstrate that our next-generation g5-HT3.0 sensor is sufficiently sensitive to monitor 5-HT release *in vivo* with high spatiotemporal resolution.

Dual-color imaging of neurochemical waves during seizure

The serotonergic system has been suggested to protect the CNS from epileptiform activity[36–39], which is characterized by excessive and hypersynchronous neuronal firing. However, little is known regarding the spatiotemporal dynamics of 5-HT release during and after seizure activity, let alone the relationship between 5-HT and other seizure-related signals such as calcium and endocannabinoid (eCB). Therefore, we employed a similar strategy as depicted in Fig. 4a to pan-neuronally co-express g5-HT3.0 together with jRGECO1a or r5-HT1.0 together with eCB2.0[40] throughout the whole brain, then performed dual-color mesoscopic imaging to measure 5-HT and calcium or eCB dynamics in the mouse dorsal cortex, while simultaneously performing EEG recording to identify seizures induced by an injection of the glutamate receptor agonist kainic acid (KA)[41] (Fig. 5a). Similar to previous reports[40, 42], we observed an increase in Ca^{2+} signals during the KA-induced seizure, followed by a spreading wave of Ca^{2+} with a larger magnitude. In the same mouse, we observed a spreading wave of 5-HT, reported by g5-HT3.0 signals, that closely followed the Ca^{2+} wave (Fig. 5b,f and Supplementary Video 1). The waves reported by g5-HT3.0 and jRGECO1a originated in approximately the same location and propagated with similar speed (at ~76 μm/s and ~83 μm/s, respectively) and in the same direction, primarily from the lateral cortex to the medial region (Fig. 5g,h). As a negative control, seizure activity had no effect on the signal measured using g5-HT3.0mut (Fig. 5c,f and Extended Data Fig. 10a,b).

Finally, we obtained similar results in mice co-expressing r5-HT1.0 and eCB2.0, with a propagating wave of 5-HT release following the eCB wave. Moreover, the waves reported by r5-HT1.0 and eCB2.0 originated in approximately the same location, propagated at similar speed (~83 μm/s and ~81 μm/s, respectively) and in the same direction (Fig. 5d,f–h and Supplementary Video 2). As above, seizure activity had no effect on the signal measured using r5-HTmut (Fig. 5e,f and Extended Data Fig. 10c,d).

Taken together, these results demonstrate that our g5-HT3.0 and r5-HT1.0 sensors can reliably report 5-HT release *in vivo* with high sensitivity, specificity, and spatiotemporal resolution both under physiological conditions and during seizure activity.

Discussion

Here, we report the development, optimization, characterization, and *in vivo* application of a series of genetically encoded red and green fluorescent 5-HT sensors. Particularly, the dual-color imaging revealed that the seizure-induced 5-HT waves were spatially correlated—but lagged behind—Ca^{2+} and eCB waves, consistent with the idea that serotonergic activity may protect against neuronal hyperactivity[36, 38]. The temporal lag between calcium and 5-HT signals indicates the possible neuromodulation of 5-HT release within serotonergic axons

following the hyperactivity of cortical neurons, but the precise mechanism underlying this delay has yet to be determined.

Our next-generation green fluorescent $GRAB_{5\text{-}HT}$ sensors have three advantages over previously reported genetically encoded fluorescent 5-HT sensors. First, g5-HT3.0 is more sensitive due to its large response, high affinity and brightness, making it more suitable for both *in vitro* and *in vivo* applications. Second, these sensors—g5-HT3.0 and g5-HT2m—spanning a range of affinities from hundred-nanomoles to micromoles, effectively bridge the critical gap in measuring intermediate concentrations of 5-HT. Specifically, the g5-HT3.0 sensor is generally suitable for detecting 5-HT dynamics across a wide range of scenarios, from modest 5-HT release (e.g., reward) to high 5-HT level changes (e.g., seizure). However, in scenarios where the 5-HT concentration is notably high, such as in the gut, g5-HT2m may offer a more appropriate detection range. Thus, together with previous sensors such as g5-HT1.0 and iSeroSnFR, users can now access a toolbox covering a wide range of physiological and pathological 5-HT concentrations[43–45]. Third, these sensors have rapid kinetics and are suitable for tracking transient 5-HT release in real time. When rapid dynamics is required, g5-HT2m is particularly suitable due to its faster sub-second off kinetics compared to g5-HT3.0 and g5-HT2h.

More importantly, our red fluorescent 5-HT sensor expands the spectral profile of genetically encoded 5-HT sensors and is suitable for dual-color imaging. We simultaneously recorded signals of r5-HT1.0 and axon-targeted GCaMP6s in the mouse BF during sleep-wake cycles and found that the two signals were closely correlated, consistent with Ca^{2+}-dependent rapid 5-HT release. Since r5-HT1.0 lacks an isosbestic point, to fully leverage the advantages of multiplex imaging with r5-HT1.0 and most green sensors, users can consider employing another spectral-compatible fluorescent protein, such as TagBFP[46], as a reference for artifact correction. Future advancements in expanding the spectra of 5-HT sensors (e.g., far-red and near-infrared) will facilitate simultaneous monitoring more neurochemicals and help disentangle their interactions with 5-HT.

When using sensors, optimizing the experimental system is crucial, which involves selecting the appropriate sensor considering various aspects, such as response, affinity and kinetics, as well as optimizing its expression level. It is also important to prevent disturbances of normal 5-HT levels. We intentionally used heterozygous *Sert-Cre* mice[28] instead of homozygotes, because the homozygous SERT-KO mice showed markedly elevated basal levels of extracellular 5-HT, whereas heterozygotes exhibited similar levels[47].

In summary, our new 5-HT sensors can monitor 5-HT release both *in vitro* and *in vivo*, with high sensitivity and spatiotemporal resolution. When combined with advanced imaging techniques, they offer a powerful toolbox to study the serotonergic system in both health and disease.

Methods

Molecular biology

Plasmids were generated via Gibson assembly[48] and verified by Sanger sequencing (RuiBiotech). For the replacement site screening, cDNAs encoding 12 different 5-HTR subtypes were cloned from the human GPCR cDNA library (hORFeome database 8.1) or the PRESTO-Tango GPCR Kit[25] (Addgene Kit #1000000068). To optimize the 5-HT sensors, cDNAs encoding candidate sensors were cloned into the pDisplay vector (Invitrogen) with an IgK leader sequence in the sensor upstream, and either IRES-mCherry-CAAX (for green fluorescent 5-HT sensors) or IRES-EGFP-CAAX (for red fluorescent 5-HT sensors) was fused downstream of the sensor to calibrate the membrane signal. Site-directed mutagenesis was performed using primers containing randomized NNB codons (48 codons in total, encoding 20 possible amino acids). For expression in cultured neurons and mice *in vivo*, sequences of sensors were cloned into the pAAV vector (AAV information provided in Supplementary Table 1). To generate stable cell lines for measuring the excitation/emission spectra, sequences encoding sensors were cloned into a vector called pPacific, containing a 3' terminal repeat, IRES, the puromycin gene, and a 5' terminal repeat. To measure downstream coupling using the Tango assay, DNA encoding various $GRAB_{5\text{-}HT}$ sensors or wild-type 5-HTR4 was cloned into the pTango vector[25]. For the luciferase complementation assay, the β_2AR gene in the β2AR-Smbit construct[24] was replaced with the indicated $GRAB_{5\text{-}HT}$ sensors or wild-type 5-HTR4; LgBit-mGs was a generous gift from Nevin A. Lambert (Augusta University).

Cell lines

HEK293T cells were purchased from ATCC (CRL-3216) and verified based on their morphology and growth rate. Stable cell lines expressing different $GRAB_{5\text{-}HT}$ sensors were generated by co-transfecting HEK293T cells with the pPacific plasmids encoding sensors and the pCS7-PiggyBAC plasmid encoding the transposase[49]. Cells expressing the desired genes were selected using 2 μg/ml puromycin (Sigma). An HTLA cell line stably expressing a tTA-dependent luciferase reporter and the β-arrestin2-TEV fusion gene used in the Tango assay[25] was a generous gift from Bryan L. Roth (University of North Carolina at Chapel Hill). All cell lines were cultured at 37 °C in 5% CO_2 in DMEM (Biological Industries) supplemented with 10% (v/v) fetal bovine serum (GIBCO) and 1% penicillin-streptomycin (GIBCO).

Primary cultures

Rat cortical neurons were prepared using postnatal day 0 (P0) Sprague-Dawley rat pups (both sexes) purchased from Beijing Vital River. The cerebral cortex was dissected, and neurons were dissociated using 0.25% trypsin-EDTA (GIBCO), plated onto 12-mm glass coverslips coated with poly-D-lysine (Sigma-Aldrich), and cultured in neurobasal medium (GIBCO) containing 2% B-27 supplement (GIBCO), 1% GlutaMax (GIBCO), and 1% penicillin-streptomycin (GIBCO) at 37 °C in humidified air containing 5% CO_2.

Animals

All procedures involving animals were performed using protocols approved by the Animal Care and Use Committee at Peking University. *Sert-Cre* mice were generously provided by Yi Rao at Peking University. All mice were group-housed or pair-housed in a temperature (18–23 °C), humidity (40–60%) and light/dark cycle (12-h/12-h) controlled room, with food and water available ad libitum.

Cell transfection and imaging

HEK293T cells were plated either on 12-mm glass coverslips in 24-well plates or 96-well plates without coverslips and grown to ~70% confluence for transfection with PEI (1 μg plasmid and 3 μg PEI per well in 24-well plates or 300 ng plasmids and 900 ng PEI per well in 96-well plates); the medium was replaced after 4–6 h, and the cells were used for imaging 24–48 h after transfection. After 5–9 d of *in vitro* culture, rat cortical neurons were infected with indicated AAVs. To compare the performance of various 5-HT sensors in Extended Data Fig. 3, each AAV was diluted to 2.53×10^{12} vg/ml and added at a volume of 1 μl/well.

Before imaging, the culture medium was replaced with Tyrode's solution consisting of (in mM): 150 NaCl, 4 KCl, 2 $MgCl_2$, 2 $CaCl_2$, 10 HEPES, and 10 glucose (pH 7.4). Cells were imaged using an inverted Ti-E A1 confocal microscope (Nikon) or an Opera Phenix high-content screening system (PerkinElmer). The confocal microscope was equipped with a 10x/0.45 NA (numerical aperture) objective, a 20x/0.75 NA objective, a 40x/1.35 NA oil-immersion objective, a 488-nm laser, a 561-nm laser and the NIS-Element 4.51.00 software; the GFP signal was collected using a 525/50-nm emission filter combined with the 488-nm laser, and the RFP signal was collected using a 595/50-nm emission filter combined with the 561-nm laser. The Opera Phenix system was equipped with a 20x/0.4 NA objective, a 40x/1.1 NA water-immersion objective, a 488-nm laser, a 561-nm laser and the Harmony 4.9 software; the GFP and RFP signals were collected using a 525/50-nm and 600/30-nm emission filter, respectively. The fluorescence signals produced by the green and red fluorescent $GRAB_{5\text{-}HT}$ sensors were calibrated using mCherry (the GFP/RFP ratio) or EGFP (the RFP/GFP ratio), respectively.

To measure the sensor responses induced by various chemicals, solutions containing indicated chemicals were administered to the cells via a custom-made perfusion system or via bath application. To measure the sensors' kinetics, a glass pipette was positioned in close proximity to cells expressing the sensors, and the fluorescence signal was measured using confocal high-speed line scanning mode with a scanning speed of 1024 Hz. To measure the on-rate constant (τ_{on}), 100 μM 5-HT was puffed from the pipette, and the increased trace in fluorescence was fitted with a single-exponential function; to measure the off-rate constant (τ_{off}), 100 μM RS 23597–190 was puffed on cells bathed in 10 μM 5-HT, and the decreased trace in fluorescence was fitted with a single-exponential function. To test for the potential photoactivation of the red fluorescent sensors mediated by blue light, cells expressing r5-HT1.0 or jRGECO1a were imaged with the inverted Ti-E A1 confocal microscope, where a 488-nm laser lasting for 1 s was utilized as the stimulation light during imaging intervals. For the photoactivation shown in Fig. 1f, cells were illuminated by a 488-nm laser emitted from the objective (power: ~210 μW, intensity: ~0.4 W/cm^2). For

results in Extended Data Fig. 1k,l, cells were illuminated by a 488-nm laser emitted from a fiber with 200-μm diameter (maximal power: ~10 mW, intensity: ~32 W/cm^2).

Spectra measurements

For 1-photon spectra, HEK293T cells stably expressing GRAB$_{5\text{-HT}}$ sensors were harvested and transferred to a 384-well plate in the absence or presence of 10 μM 5-HT. Excitation and emission spectra were measured at 5-nm increments with a 20-nm bandwidth using a Safire2 multi-mode plate reader (Tecan). Non-transfected cells were prepared to the same density as the cells that expressed sensors, and were measured using the same protocol for background subtraction.

For 2-photon spectra, HEK293T cells expressing sensors were cultured on 12-mm coverslips and imaged using a 2-photon microscope. The 2-photon excitation laser was measured at 10-nm increments, and laser power was calibrated for various wavelengths. For green sensors, excitation spectra were measured ranging from 690 to 1030 nm using an Ultima Investigator 2-photon microscope (Bruker) equipped with a 20x/1.0 NA water-immersion objective (Olympus), an InSight X3 tunable laser (Spectra-Physics) and the Prairie View 5.5 software (Bruker). For the red sensor, excitation spectra were measured ranging from 820 to 1300 nm using an A1R MP+ multiphoton microscope (Nikon) equipped with a 25x/1.1 NA objective (Nikon) and a Chameleon Discovery tunable laser (Coherent).

Luciferase complementation assay

The luciferase complementation assay was performed as previously described[24]. In brief, 24–48 h after transfection, the cells were washed with PBS, dissociated using a cell scraper, resuspended in PBS, transferred to opaque 96-well plates containing 5 μM furimazine (NanoLuc Luciferase Assay, Promega), and bathed in 5-HT at various concentrations (ranging from 0.01 nM to 1 mM). After incubation for 10 minutes in the dark, luminescence was measured using a VICTOR X5 multilabel plate reader (PerkinElmer).

Tango assay

A reporter cell line called HTLA, stably expressing a tTA-dependent luciferase reporter and a β-arrestin2-TEV fusion gene, was transfected with pTango vectors to express GRAB$_{5\text{-HT}}$ sensors or wild-type 5-HTR4 or both GRAB$_{5\text{-HT}}$ sensors and 5-HTR4. After culturing for 24 h in 6-well plates, the cells were transferred to 96-well plates and bathed with 5-HT at varying concentrations (ranging from 0.01 nM to 100 μM). The cells were then cultured for 12 h to allow the expression of tTA-dependent luciferase. Bright-Glo reagent (Fluc Luciferase Assay System, Promega) was added to a final concentration of 5 μM, and luminescence was measured using a VICTOR X5 multilabel plate reader (PerkinElmer).

Behavior assays

Wild-type male C57BL/6J mice (6–8 weeks of age) were anesthetized with an i.p. injection of tribromoethanol (Avertin; 500 mg/kg body weight) and placed on a stereotaxic frame (RWD Life Science). Then 400 nl indicated AAVs (diluted to 1.86 × 10^{13} vg/ml) were unilaterally injected into the basal amygdala (BA) with the following coordinates: AP: −1.35 mm relative to Bregma; ML: +/− 3.0 mm; DV: 4.5 mm below the dura, via a glass

pipette using a micro-syringe pump (Nanoliter 2000 Injector, World Precision Instruments). Three weeks later, the same cohort of mice was subjected to various behavioral tests in the following order: elevated plus maze test, tail suspension test and forced swimming test. The behavior analysis was performed using the Smart 3.0 (Panlab) software.

Elevated plus maze test.—The elevated plus maze is comprised of two opposite open arms (30 cm × 5 cm) without walls, two closed arms (30 cm × 5 cm × 15 cm) with opaque walls and these four arms are connected by a central platform (5 × 5 cm). The maze is elevated 50 cm above the floor. At the beginning of each session, mice were placed in the center zone facing one of the open arms, and were allowed to explore the maze for 5 min. Locomotion trajectories were recorded by a video camera. The arena was thoroughly cleaned with 75% ethanol between subjects. The time and entries in different zones were quantified and analyzed.

Tail suspension test.—The mouse was suspended by the tail ~40 cm above the floor, preventing any other contact or climbing during the assay. Then, a 6-min session was recorded and immobility time during 2–6 min was analyzed.

Forced swimming test.—The mouse was placed in a transparent cylinder (12 cm in diameter and 30 cm in height) filled with water to a depth of 15 cm and maintained at 23–24 °C for a 6-min session recording. After each session, the mouse was dried with paper towels and returned to its home cage. The total immobility time during 2–6 min was analyzed. Mice were considered immobile when they did not make any active movements.

Fluorescence imaging of sensors in mouse acute brain slices

Wild-type male C57BL/6J mice (6–8 weeks of age) were anesthetized with an i.p. injection of tribromoethanol (Avertin; 500 mg/kg body weight) and placed on a stereotaxic frame. Then the mixture of AAV9-hSyn-g5-HT3.0 (300 nl) and AAV9-hSyn-rDA3m (300 nl) was injected into the DRN (AP: −4.1 mm relative to Bregma; ML: +1.1 mm; depth: 2.9 mm below the dura; at a 20° ML angle) at a rate of 50 nl/min. Three weeks after AAV injection, the mice were deeply anesthetized with Avertin and perfused with 10 ml ice-cold oxygenated slicing buffer containing (in mM): 110 choline-Cl, 2.5 KCl, 0.5 $CaCl_2$, 7 $MgCl_2$, 1 NaH_2PO_4, 25 $NaHCO_3$, 25 glucose, 1.3 sodium ascorbate and 0.6 sodium pyruvate. Mice were then decapitated, and brains were rapidly removed and placed in cold (0–4 °C) oxygenated slicing buffer for an additional 1 min. Next, brains were dissected for mounting to the cutting stage, and 300-μm thick coronal slices were cut in ice-cold oxygenated slicing buffer using a VT1200 vibratome (Leica). The slices containing DRN were transferred and allowed to recover for at least 40 min at 34 °C in oxygenated artificial cerebrospinal fluid (ACSF) containing (in mM): 125 NaCl, 2.5 KCl, 2 $CaCl_2$, 1.3 $MgCl_2$, 1 NaH_2PO_4, 25 $NaHCO_3$, 25 glucose, 1.3 sodium ascorbate and 0.6 sodium pyruvate. For dual-color confocal imaging, the brain slices were then transferred to a custom-made perfusion chamber and imaged using an LSM710 confocal microscope (Zeiss), equipped with a 20x/0.5 NA water-immersion objective and the ZEN 2012 (Version 11.0.4.190) software. To minimize the spectral mixing, g5-HT3.0 and rDA3m were excited by a 488-nm laser and a 543-nm laser sequentially. The g5-HT3.0 and rDA3m signals were collected

using the detection wavelength ranging from 509 nm to 558 nm and 580 nm to 649 nm, respectively. For electrical stimulation, a homemade bipolar electrode (WE30031.0A3, MicroProbes) was placed onto the surface of the brain slice near the DRN expressing sensors. Electrical stimuli were applied using an S48 stimulator (Grass Instruments), with a stimulation voltage of 5–8 V and pulse duration of 1 ms. And the frame scan was set to a size of 256 × 192 pixels with a speed of ~0.295 s per frame. For the spontaneous transients, the frame scan was set to a size of 512 × 512 pixels with a speed of ~1 s per frame and the duration of each session was ~10 min.

Data of electrical stimuli was analyzed using custom programs written in ImageJ Macros and MATLAB. Data of spontaneous transients was preprocessed with Astrocyte Quantitative Analysis (AQuA)[50], then analyzed using custom-written MATLAB programs and ImageJ Macros.

Fiber photometry recording of optogenetically evoked 5-HT release *in vivo*

To express the red fluorescent 5-HT sensors in the BF, adult *Sert-Cre* mice were anesthetized with 1.5% isoflurane and placed on a stereotaxic frame. AAV9-hSyn-r5-HT1.0 or AAV9-hSyn-r5-HTmut was injected (400 nl) into the BF at the following coordinates: AP: 0 mm relative to Bregma; ML: +1.5 mm; DV: 4.6 mm below the dura. For optical activation of the DRN, 400 nl AAV9-EF1a-DIO-hChR2(H134R)-EYFP was injected into the DRN at the following coordinates: AP: −4.1 mm relative to Bregma; ML: +1.1 mm; depth: 2.9 mm below the dura; at a 20° ML angle. Two optical fiber cannulas (200 μm, 0.37 NA, Inper) were then implanted; one cannula was implanted 0.1 mm above the virus injection site in the BF to record the 5-HT sensor signals, and the other cannula was implanted 0.3 mm above the virus injection site in the DRN for optically activating ChR2. The optical fibers were affixed to the skull surface using dental cement. The fiber photometry system (Inper) was used to record the fluorescence signals in freely moving mice. Yellow light-emitting diode (LED) light was bandpass filtered (561/10 nm), reflected by a dichroic mirror (495 nm), and then focused using a 20x objective lens (Olympus). An optical fiber was used to guide the light between the commutator and the implanted optical fiber cannulas. The excitation light emitted by the LED was adjusted to 20–30 μW and delivered at 10 Hz with a 20-ms pulse duration. The optical signals were then collected through the optical fibers. Red fluorescence was bandpass filtered (520/20 nm and 595/30 nm) and collected using an sCMOS camera. To induce ChR2-mediated 5-HT release, pulse trains (10-ms pulses at 50 Hz for 1 s, 5 s, or 10 s) were delivered to the DRN using a 488-nm laser at 10 mW with a 5-min inter-stimulus interval. To test the effects of fluoxetine on the ChR2-induced responses, three optical stimulation trains were applied at a 5-min interval. Then, 10 mg/kg fluoxetine was administered via i.p. injection; 30 min after injection, three optical stimulation trains were applied.

The current output from the photomultiplier tube was converted to a voltage signal using a model 1700 differential amplifier (A-M Systems) and passed through a low-pass filter. The analog voltage signals were then digitized using an acquisition card (National Instruments). To minimize autofluorescence of the optical fibers, the recording fibers were photobleached

using a high-power LED before recording. Background autofluorescence was recorded and subtracted from the recorded signals in the subsequent analysis.

The photometry data were analyzed using a custom program written in MATLAB. To calculate $\Delta F/F_0$ during the optogenetics experiments, a baseline was measured before optical stimulation.

Fiber photometry recording of 5-HT dynamics during the sleep-wake cycle

Adult wild-type C57BL/6 mice or *Sert-Cre* mice were anesthetized with isoflurane and placed on a stereotaxic frame for AAV injection (400 nl per site). In Fig. 3f–g, AAV9-hSyn-r5-HT1.0 or AAV9-hSyn-r5-HTmut was injected into the BF, and EF1α-DIO-axon-GCaMP6s was injected into the DRN of *Sert-Cre* mice. In Extended Data Fig. 7a–c, AAV9-CAG-g5-HT1.0, diluted to 3.16×10^{12} vg/ml, was injected into the BF in one hemisphere, and AAV9-CAG-g5-HT3.0 was injected into the BF in another hemisphere using the coordinates described above. In Extended Data Fig. 7d–f, AAV9-hSyn-PsychLight2 and AAV9-hSyn-g5-HT3.0 (diluted to 3.07×10^{12} vg/ml) were injected into the bilateral BF, respectively. In Extended Data Fig. 7g–i, AAV9-CAG-iSeroSnFR and AAV9-CAG-g5-HT3.0 (diluted to 2.15×10^{12} vg/ml) were injected into the bilateral BF, respectively. In Extended Data Fig. 7, wild-type C57BL/6 mice were used. An optical fiber cannula (200 μm, 0.37 NA, Inper) was implanted 0.1 mm above the virus injection site in BF for recording sensor signals.

To assess the impact of viral titer on sensors' performance *in vivo* (Supplementary Fig. 2), according to the highest viral titers in our hands, AAVs with indicated titers (including high, medium and low titer) were injected into the bilateral BF as described above.

To record the animal's sleep-wake state, we attached and fixed custom-made EEG and EMG electrodes to the skull via a microconnector. EEG electrodes were implanted into craniotomy holes situated over the frontal cortex and visual cortex, and EMG wires were placed bilaterally in the neck musculature. The microconnector was attached to the skull using glue and a thick layer of dental cement. After surgery, the mice were allowed to recover for at least 2 weeks.

The same fiber photometry system (Inper) was used to record the fluorescence signals in freely moving mice during sleep-wake cycles. In Fig. 3f,g, a 10-Hz 470/10-nm filtered light (20–30 μW) was used to excite the green fluorescent calcium sensor, and a 561/10-nm filtered light (20–30 μW) was used to excite the red fluorescent 5-HT sensors. Fluorescence signals were collected using a dual-band bandpass filter (520/20 nm and 595/30 nm), with excitation light delivered as 20-ms pulses at 10 Hz. In Extended Data Fig. 7, a 10-Hz 470/10-nm filtered light (20–30 μW) was used to excite green fluorescent 5-HT sensors, and a 520/20-nm and 595/30 nm dual-band bandpass filter was used to collect the fluorescence signals.

Photometry data were analyzed using a custom MATLAB program. To calculate the $\Delta F/F_0$ during sleep-wake cycles, baseline values were measured during a period of REM sleep in which no apparent fluctuations were observed. To better quantify the fluorescence changes

across multiple animals, the $\Delta F/F_0$ was further normalized using the s.d. of the baseline signals to get the *z*-score, with the formula: *z*-score = $\Delta F/F_0$ / $s.d._{baseline}$.

Fiber photometry recording of 5-HT dynamics during reward, sensory stimuli, and punishment conditions

Adult wild-type C57BL/6 mice were anesthetized with isoflurane and placed on a stereotaxic frame. In Extended Data Fig. 8a–d, AAV9-CAG-g5-HT1.0 (diluted to 3.16×10^{12} vg/ml) and CAG-g5-HT3.0 were injected bilaterally into the basal amygdala (BA) with 400 nl per site at the following coordinates: AP: −1.35 mm relative to Bregma; ML: +/− 3.0 mm; DV: 4.5 mm below the dura. In Extended Data Fig. 8e–g, AAV9-CAG-iSeroSnFR and CAG-g5-HT3.0 (diluted to 2.15×10^{12} vg/ml) were injected into the bilateral BA (400 nl per site), respectively. An optical fiber cannula (Inper) was implanted 0.1 mm above the virus injection sites in BA for recording the signals of 5-HT sensors.

Reward.—Intraoral cheek fistula was implanted and several days were allowed for the recovery of the mice. Mice were water restricted for 36 h (to 85% of initial body weight). Then water-restricted freely moving mice received 5% glucose water delivery (around 10 ul per trial; 10 trials per session, trial interval between 20–30 s).

Tone.—The mouse was placed in a box with a loudspeaker, and 2-second tone (5 kHz, 70 dB) was delivered for 10 trials with a 30-s interval between trials.

The same fiber photometry system (Inper) was used to record the fluorescence signals in freely moving mice during the sleep-wake cycle. In Extended Data Fig. 8, a 10-Hz 470/10-nm filtered light (20–30 μW) was used to excite green fluorescent 5-HT sensors. A 10-Hz 410/10-nm filtered light (20–30 μW) served as a control channel.

The fluorescence intensity of green 5-HT sensors excited by 410 nm and 470 nm was recorded as F_{410} and F_{470}, respectively. The $\Delta F/F_0$ was calculated during the above conditions using the formula: $\Delta F/F_0 = \Delta(F_{470}/F_{410}) / (F_{470}/F_{410})$. Baseline values were determined before the application of various stimuli. The z-score was computed as: *z*-score = $\Delta(F_{470}/F_{410}) / (F_{470}/F_{410}) / s.d._{baseline}$.

Polysomnographic recording and analysis

The animal's sleep-wake state was determined using the EEG and EMG recordings. The EEG and EMG signals were amplified (NL104A, Digitimer), filtered (NL125/6, Digitimer) at 0.5–100 Hz (EEG) and 30–500 Hz (EMG), and then digitized using a Power1401 digitizer (Cambridge Electronic Design Ltd.). The Spike2 software program (Cambridge Electronic Design Ltd.) was used for recording with a sampling rate of 1000 Hz. The animal's sleep-wake state was classified semi-automatically in 4-s epochs using AccuSleep[51] and then validated manually using a custom-made MATLAB GUI. The wake state was defined as desynchronized EEG activity combined with high EMG activity. NREM sleep was defined as synchronized EEG activity with high-amplitude delta activity (0.5–4 Hz) and low EMG activity. REM sleep was defined as high-power theta frequencies (6–9 Hz) combined with low EMG activity.

Mesoscopic *in vivo* imaging

To express the sensors throughout the cortex, we injected the indicated AAVs into the transverse sinus as described previously[32]. In detail, P0–P1 C57BL/6 mouse pups were removed from their home cages, placed on a warm pad, anesthetized on ice for 2–3 min, and fixed on an ice cooled metal plate. Two small incisions were then made over the transverse sinuses for AAV injection using a glass pipette. For single-color imaging in the optogenetic experiments, AAV9-hSyn-g5-HT3.0 or AAV9-hSyn-EGFP-CAAX was injected bilaterally (4 μl total volume, 2 μl per hemisphere). For dual-color imaging, the pups were injected bilaterally with the following pairs of AAVs (6 μl total volume, 1:1): AAV9-hSyn-g5-HT3.0 and AAV9-hSyn-GAP43-jRGECO1a; AAV9-hSyn-r5-HT1.0 and AAV9-hSyn-eCB2.0; AAV9-hSyn-g5-HT3.0mut and AAV9-hSyn-GAP43-jRGECO1a; or AAV9-hSyn-r5-HTmut and AAV9-hSyn-eCB2.0. The AAVs were injected at a rate of 1.2 μl/min, and the pipette was left in the sinus for at least 30 s. After injection, the incisions were sealed with Vetbond glue (3M Animal Care Products) and the pups were placed on a warm pad for recovery. After recovery, the pups were gently rubbed with bedding and returned to their home cage.

About eight weeks after AAV injection, surgery was performed for implanting the imaging window and the EEG and EMG electrodes. Anesthesia was induced with an i.p. injection of 2,2,2-tribromoethanol (Avertin, 500 mg/kg, Sigma-Aldrich) and maintained using inhalation with 1% isoflurane. The mouse was fixed in a stereotaxic frame, 2% lidocaine hydrochloride was injected under the scalp, and the eyes were covered with erythromycin ophthalmic ointment for protection. Part of the scalp above the skull and the underlying muscles were removed and cleaned carefully to expose the skull. Most of the skull above the dorsal cortex was then carefully removed and replaced with a flat custom-made coverslip (D-shape, ~8 mm × 8 mm) to create an optical window. EEG and EMG electrodes were implanted and fixed as described above. After surgery, the mice were returned to their home cage for at least 7 d to recover, and then fixed to the base for over 3 d to habituate before imaging until the mouse can fall asleep (especially REM sleep) within the first 3 h. To optically activate the DRN, we used *Sert-Cre* mice. As described above, except before the surgery, 300 nl AAV9-EF1a-DIO-ChrimsonR-iP2A-Halotag9-V5 was injected into the DRN using the following coordinates: AP: −6.1 mm relative to Bregma; ML: 0 mm relative to Bregma; depth: 3 mm below the dura; at a 32° AP angle (to avoid the imaging window, the fiber is inserted forward and down from the back of the interparietal bone). An optical fiber cannula (Inper) was then implanted 0.2 mm above the virus injection site and affixed to the skull surface using dental cement.

Mesoscopic imaging was performed using a custom-made dual-color macroscope equipped with a 2x/0.5 NA objective lens (Olympus, MVPLAPO2XC), two 1x/0.25 NA tube lenses (Olympus, MVPLAPO1X), and two sCMOS cameras (Andor, Zyla 4.2 Plus, 2,048×2,048 pixels, 16-bit)[52, 53]. Three excitation wavelengths (405 nm, 488 nm, and 561 nm) were generated using a multi-line fiber coupled laser system (Changchun New Industries Optoelectronics Tech. Co., Ltd., RGB-405/488/561/642nm-220mW-CC32594). The emission light was passed through a 567-nm cut-on longpass dichroic mirror (Thorlabs, DMLP567L), then through either a 525/36-nm or 609/34-nm emission filter (Chroma) into

the sCMOS cameras. Both the excitation laser and the camera imaging were triggered by an Arduino board (Uno) with custom-written programs. Images were acquired using the Micro-Manager 2.0 software (NIH). For green sensor imaging, a 488-nm laser was used and interleaved with a 405-nm laser; while for dual-color imaging, 488-nm and 561-nm lasers were simultaneously generated and interleaved with a 405-nm laser. Images were acquired using Micro-Manager 2.0 at a resolution of 512 × 512 pixels after 4× pixel binning, and each channel was acquired at either 1 Hz or 5 Hz with 40-ms exposure.

During imaging, the mice were head-fixed to the base and could freely run on a treadmill[54]. To induce ChrimsonR-mediated 5-HT release in the optogenetics experiment, pulse trains of light (10-ms pulses for 10 s at 5, 10, 20, 30, 40, or 50 Hz) were applied to the DRN using a 635-nm laser at 10 mW with a 3-minute interval, and three trials were performed at each frequency. To test the effects of fluoxetine and GBR 12909 on ChrimsonR-evoked 5-HT release, three trains of optical stimulation (10-ms pulses for 1 s at 20 Hz, 10-ms pulses for 10 s at 20 Hz, or 10-ms pulses for 10 s at 50 Hz) were applied with a 5-min interval, and three trials were conducted for each parameter. Then, 10 mg/kg GBR 12909 was injected i.p., and the same optical stimulation procedure was performed 30 min later. Next, 20 mg/kg fluoxetine was injected i.p., followed by the same optical stimulation procedure 30 min later (see Extended Data Fig. 9a). For the seizure experiments, an infrared camera was hung above the back of the mouse to record its behavioral data. After recording ~1 h of baseline data, 10 mg/kg KA was injected i.p. to induce seizures. All recordings, including mesoscopic imaging, EEG and EMG recording, optical stimulation trains, and the infrared cameras, were synchronized using a Power1401 acquisition board (Cambridge Electronic Design Ltd.).

Analysis of mesoscopic imaging data

Preprocessing.—Raw images acquired by each camera were calibrated for the uniformity of the imaging system, and movement-related artifacts were corrected using the motion-correction algorithm NoRMCorre (ref.[55]). The corrected image stack with a size of 512 × 512 pixels was downsampled by a factor of 0.7 to 359 × 359 pixels for subsequent analysis. For dual-color imaging, the averaged red-channel image was registered to the averaged green-channel image via automatic transformation using the MATLAB function “imregtform” with the “similarity” mode. The same geometric transformation was applied to all red-channel images to register to corresponding green-channel images. The image stack was saved as a binary file to accelerate the input and output of large files (typically >8 GB). To remove pixels belonging to the background and blood vessels (particularly large veins), we generated a mask for further analysis of the pixels. Specifically, the outline of the entire dorsal cortex in the field of view was generated manually, and pixels outside the outline were set as background and excluded from further analysis. The blood vessels were then removed from the image using the machine learning-based ImageJ plugin Trainable Weka Segmentation[56] (v3.3.2) in order to minimize artifacts caused by the constriction and dilation of blood vessels. The final mask without the background and blood vessel pixels was applied to the image stack for further analysis.

Spectral unmixing.—For simultaneous dual-color imaging, the bleed-through of fluorescence intensity for each pixel between the green and red channels was removed using linear unmixing[57] based on the spectra of the various sensors and the setup of the microscope system. Specifically, the proportion of fluorescence intensities detected by two cameras for various sensors was calculated based on sensors' emission spectra and the bandpass of filters. The value of each pixel in preprocessed images was recalculated based on these ratios for linear unmixing with following equations:

$$F_{G'} = F_G + F_R \times C_G \quad ①$$

$$F_{R'} = F_R + F_G \times C_R \quad ②$$

Where F_G and F_R indicate the real fluorescence intensity of the pixel in green and red channel, respectively; $F_{R'}$ and $F_{R'}$ indicate the measured fluorescence intensity of the pixel in green and red channel, respectively; C_G and C_R indicate the bleed-through ratio in green channel (from red sensors) and red channel (from green sensors), respectively. And we can get the exact value F_G and F_R based on other values including $F_{R'}$, $F_{R'}$, C_G and C_R with following formulas:

$$F_G = (F_{G'} - F_{R'} \times C_G)/(1 - C_G \times C_R) \quad ③$$

$$F_R = (F_{R'} - F_{G'} \times C_R)/(1 - C_G \times C_R) \quad ④$$

The images after spectral unmixing were used for further analysis.

Hemodynamic correction and response calculation.—Hemodynamic changes can affect the absorption of light, resulting in changes in fluorescence[58, 59]. According to the spectra of the sensors, when excited with 405-nm light, the g5-HT3.0, eCB2.0, r5-HT1.0, and jRGECO1a sensors are ligand-insensitive, which can reflect hemodynamic absorption. To correct for hemodynamic artifacts, we performed a pixel-by-pixel correction based on linear regression[60] of the ligand-dependent signals (excited by 488 nm or 561 nm) against the ligand-independent signals (excited by 405 nm). The baseline images were spatially smoothed using a Gaussian filter ($\sigma = 2$) and used for the linear regression. Then, for each pixel, the baseline fluorescence intensity of the 405-nm excited channel was regressed onto the 488-nm or 561-nm signal, obtaining regression coefficients for rescaling the 405-nm channel. The rescaled 405-nm signal was subtracted from the 488-nm or 561-nm signal to generate a corrected signal for each pixel. To avoid the corrected signal becoming close to zero or even less than zero, the corrected signal was added to the average

rescaled 405-nm channel signal as the final corrected signal of fluorescence intensity for the response calculation. The response of each pixel was calculated using the equation $\Delta F/F_0 = (F-F_0)/F_0$, where F_0 is defined as the average baseline fluorescence intensity. When analyzing the data obtained during sleep-wake cycles, the baseline was defined as the REM sleep state, in which the signal had no apparent fluctuation.

Parcellation of cortical areas.—Based on previous studies[61, 62], we rigidly registered the average fluorescence image to a 2D projection of the Allen Common Coordinate Framework v3 (CCFv3) using four manually labeled anatomical landmarks, namely the left, center, and right points in the boundary between the anterior cortex and the olfactory bulbs, and the medial point at the base of the retrosplenial cortex. To analyze the time series response in an individual brain region, we averaged the $\Delta F/F_0$ value for all available pixels within that brain region. To obtain the average response map from multiple mice (see Fig. 4g), we developed a custom code that first register the response image for each individual mouse to the Allen CCFv3, and then averaged the images, keeping only the intersection among all mice. For the analysis of serotonergic projection in the mouse dorsal cortex, the serotonergic projection map was modified from Allen Mouse Brain Connectivity Atlas, connectivity.brain-map.org/projection/experiment/cortical_map/480074702.

Analysis of propagating waves

Peak response calculation.—The time series of the images obtained before (~30 s before the wave originated), during, and after (~30 s after the wave disappeared) wave propagation was extracted as an event for further analysis. Images taken during the first 20 s (20 frames) were set as the event baseline. The event response image was spatially filtered, and each pixel during the event was then corrected to set the average response of the event baseline to zero. The peak response site was automatically found by a circle with a 500-μm diameter across the event, and its average value was defined as the peak response of the event.

Identification of wave directions using optical flow analysis.—To determine the direction of the waves, we adopted an optical flow method for automatically detecting the wave directions based on the NeuroPatt toolbox[63]. In detail, the corrected response image stack was smoothed over time, downsampled in size by a factor of 0.2, and normalized to the maximum response for each pixel. The phase velocity fields were then calculated using the “opticalFlowHS” MATLAB function (smoothness parameter $\alpha = 0.05$). For each frame, velocity fields were ignored in pixels with a low response, defined as smaller than threefold s.d. of the baseline. Finally, we obtained the frequency distribution of these wave directions in each event and the average distribution of all events (see Fig. 5h).

Calculation of wave speed.—The velocity fields calculated using the optical flow method depend on two parameters[63] and tend to be underestimated; therefore, we used a different method to calculate the speed of waves (see Extended Data Fig. 10e). In detail, the time (T) to peak response for each pixel was determined, and the pixel with the shortest time (T_0) to reach the peak response was defined as the origin. The wave-propagating region was then divided by fans centered at the origin with 0.5° intervals, and the relative distance

(ΔS) between the distal pixel and the origin was calculated. The speed (v) in each direction was then calculated using the equation $v = \Delta S/(T-T_0)$. Finally, we obtained the frequency distribution for speed in each event and the average distribution of all events (see Fig. 5h).

Quantification and statistical analysis

Where appropriate, cells or animals were randomly assigned to either the control or experimental group. Imaging data were processed using ImageJ (1.53q) software (NIH) and custom-written MATLAB (R2020b) programs. Data were plotted using OriginPro 2020b (Originlab) or Adobe Illustrator CC. Except where indicated, otherwise, all summary data are reported as the mean ± SEM. The SNR was calculated as the peak response divided by the s.d. of the baseline fluorescence fluctuation. All data were assumed to be distributed normally, and equal variances were formally tested. Differences were analyzed using the two-tailed Student's *t*-test or one-way ANOVA; $*P<0.05$, $**P<0.01$, $***P<0.001$, and n.s., not significant ($P\geq0.05$).

Extended Data

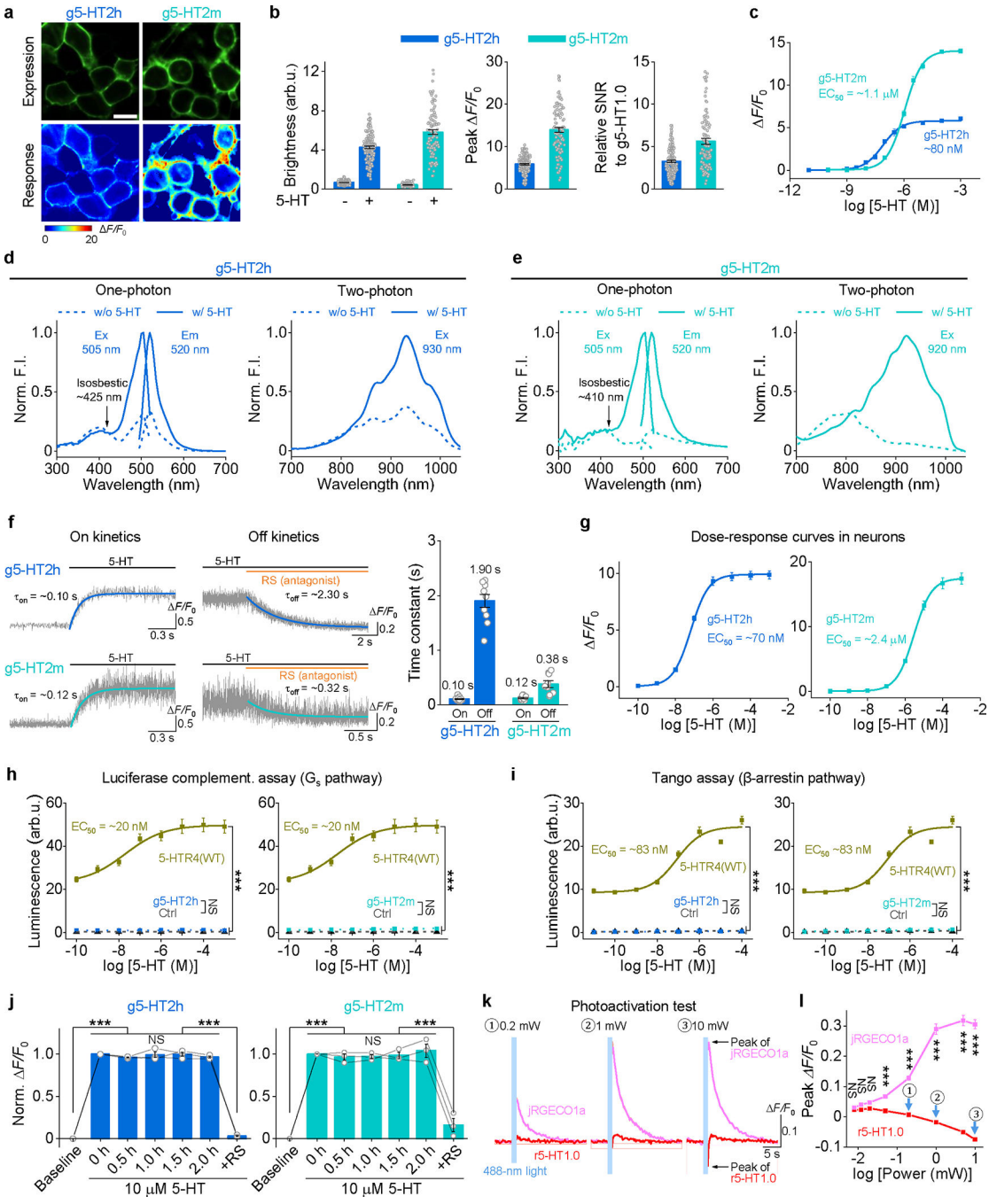

Extended Data Fig. 1 |. Characterization of GRAB$_{5\text{-}HT}$ sensors in HEK293T cells and cultured rat cortical neurons.

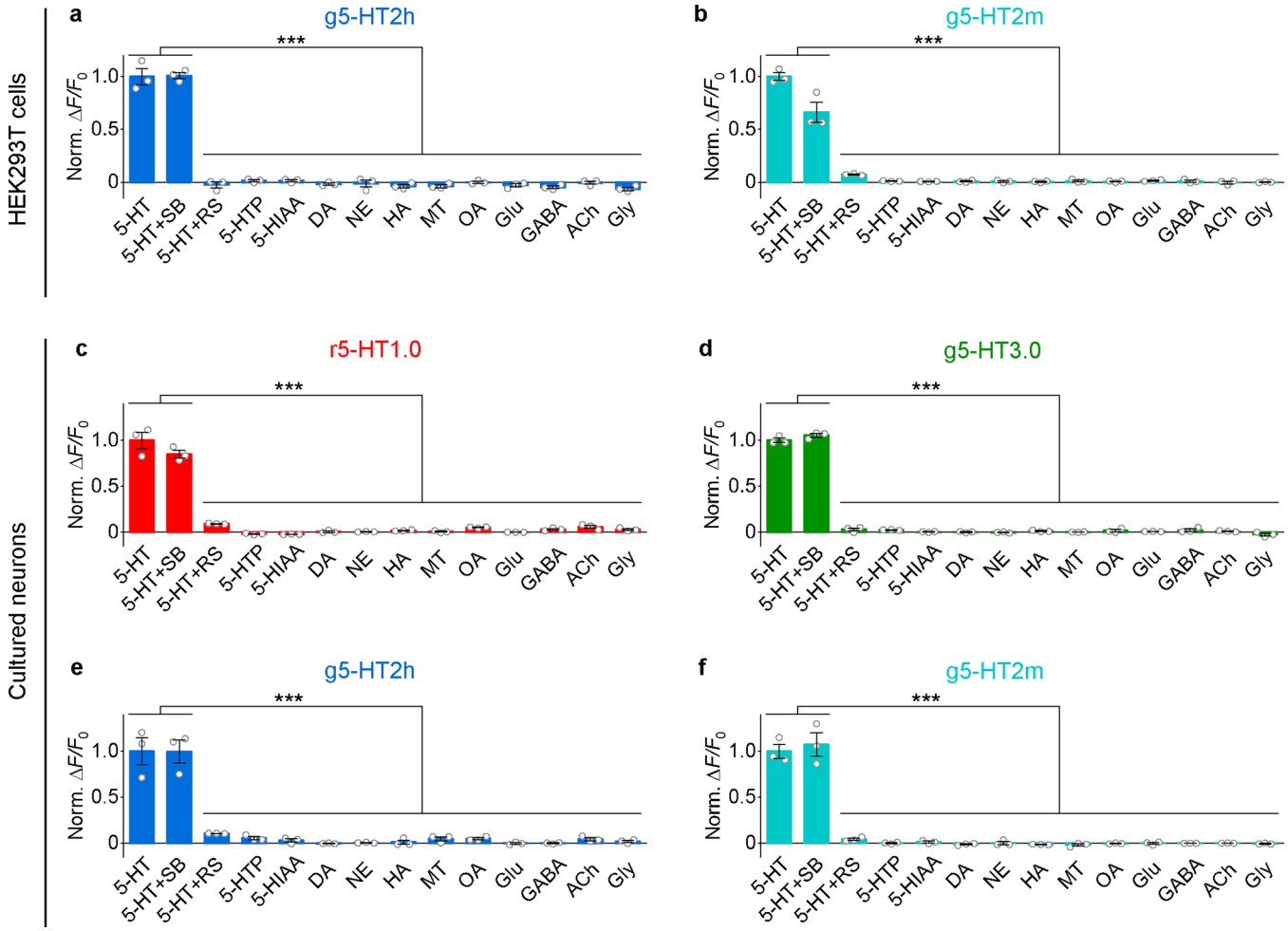

Extended Data Fig. 2 |. Specificity of 5-HT sensors.

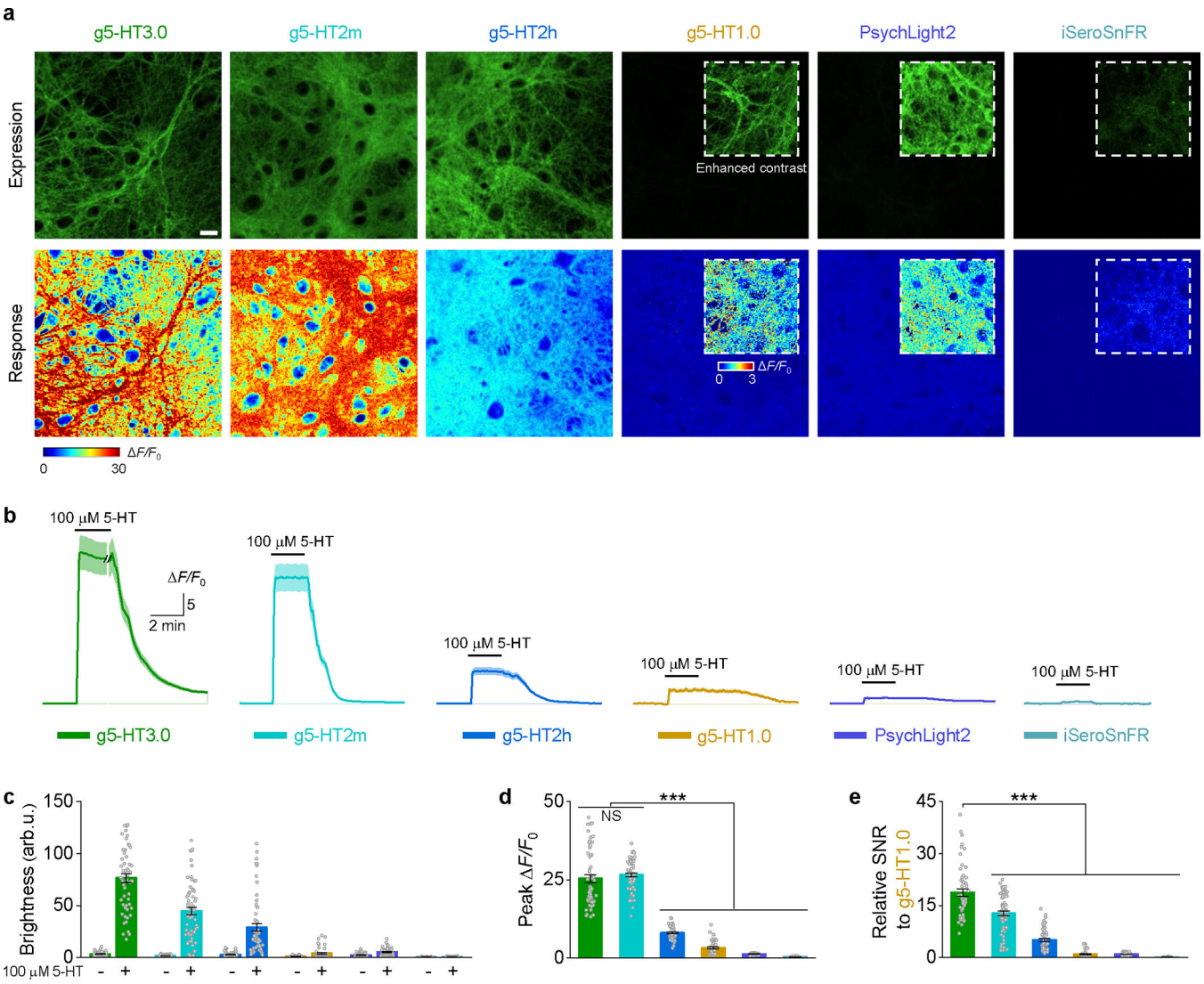

Extended Data Fig. 3 |. Comparison of single GFP-based 5-HT sensors in cultured rat cortical neurons.

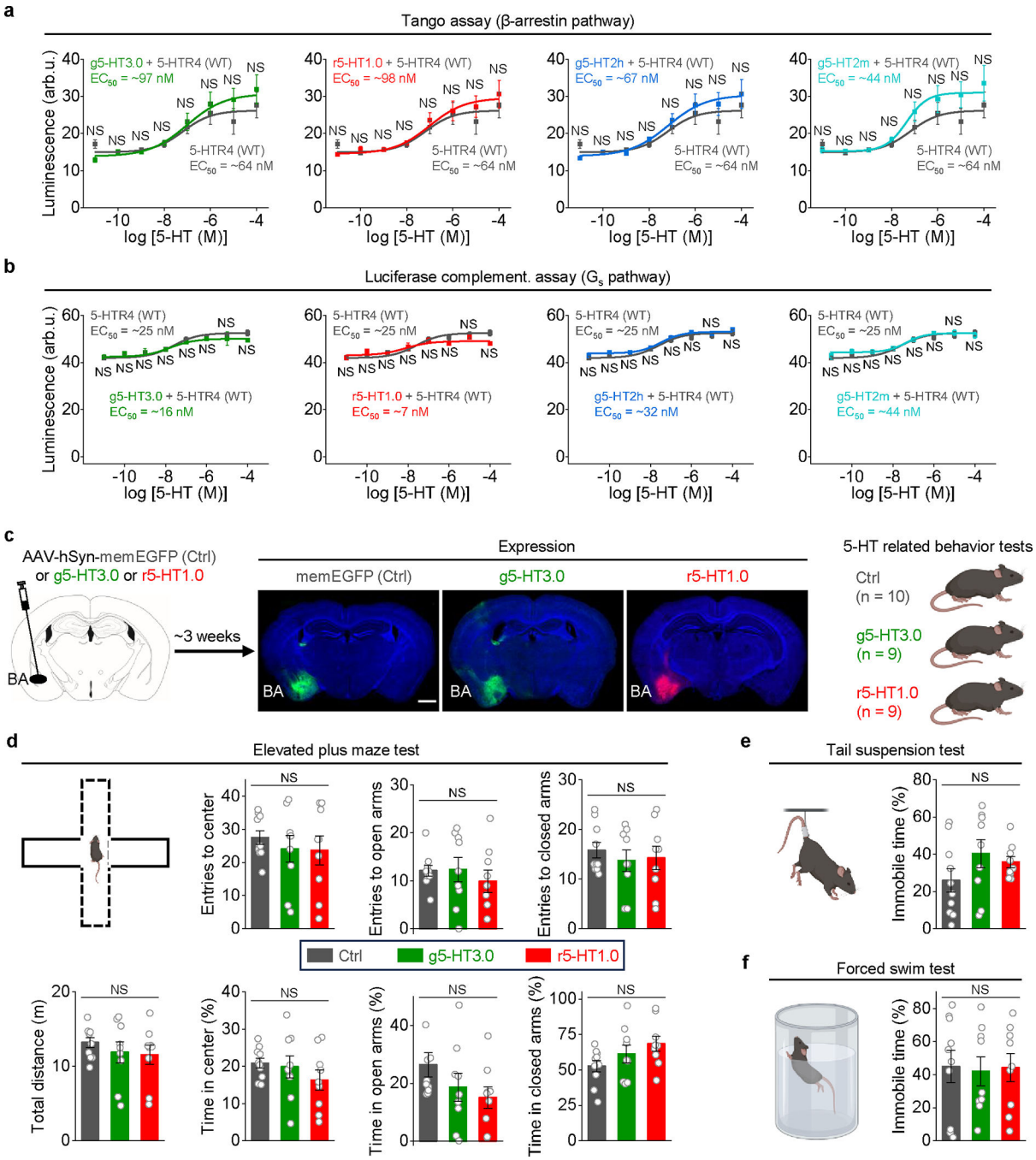

Extended Data Fig. 4 |. Expression of GRAB$_{5\text{-}HT}$ sensors shows minimal buffering effects.

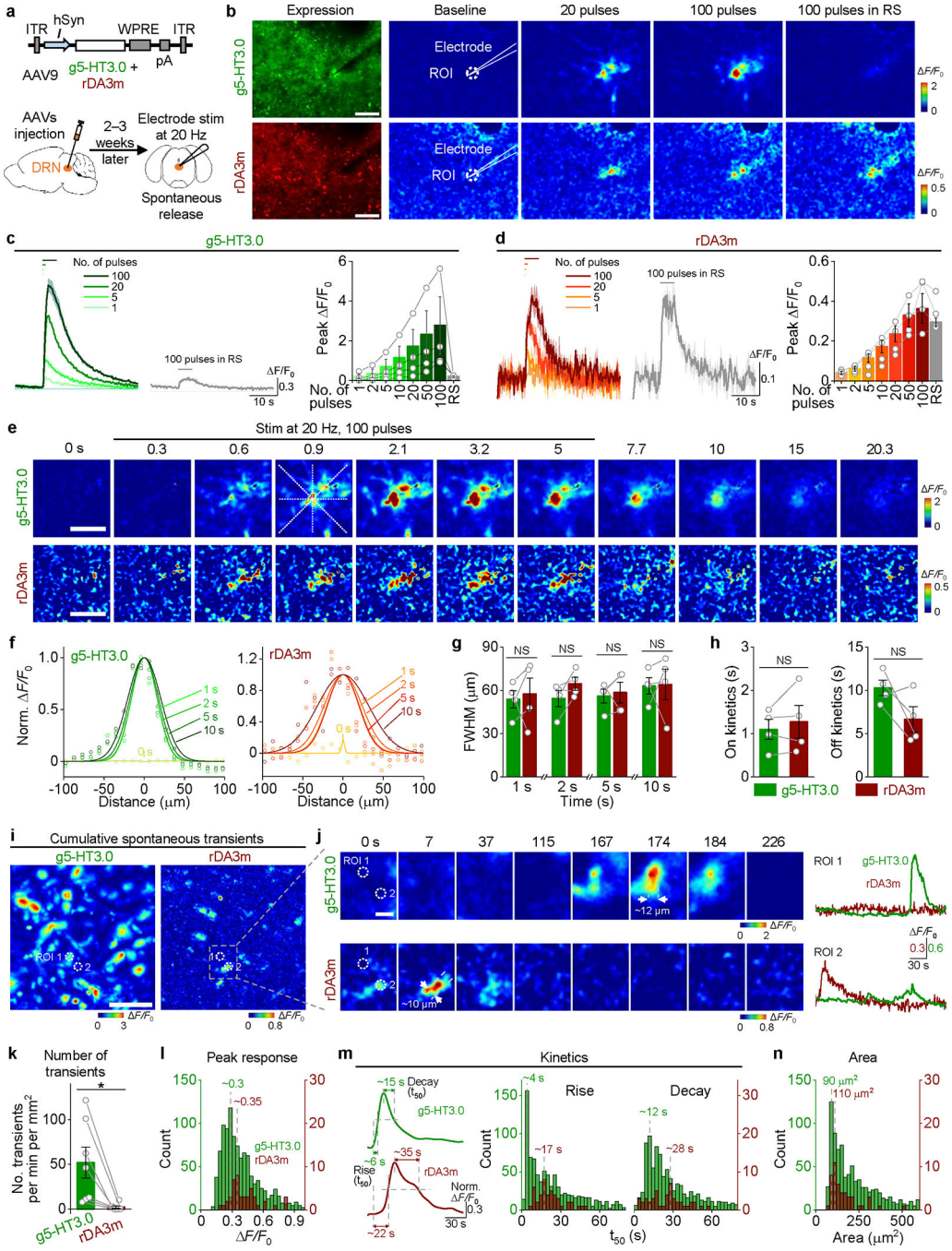

Extended Data Fig. 5 |. Dual-color imaging of 5-HT and DA dynamics in acute mouse brain slices with high spatial-temporal resolution.

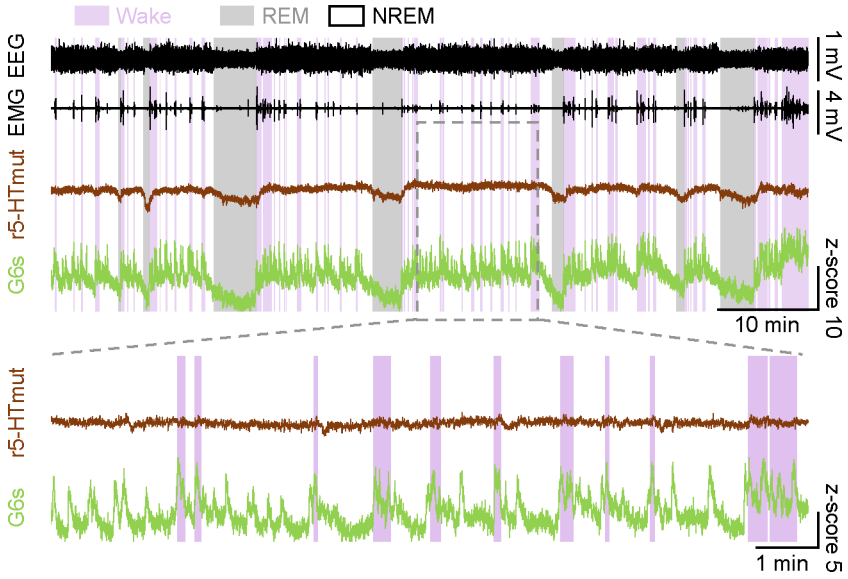

Extended Data Fig. 6 |. Representative r5-HTmut and GCaMP6s signals during the sleep-wake cycle in freely moving mice.

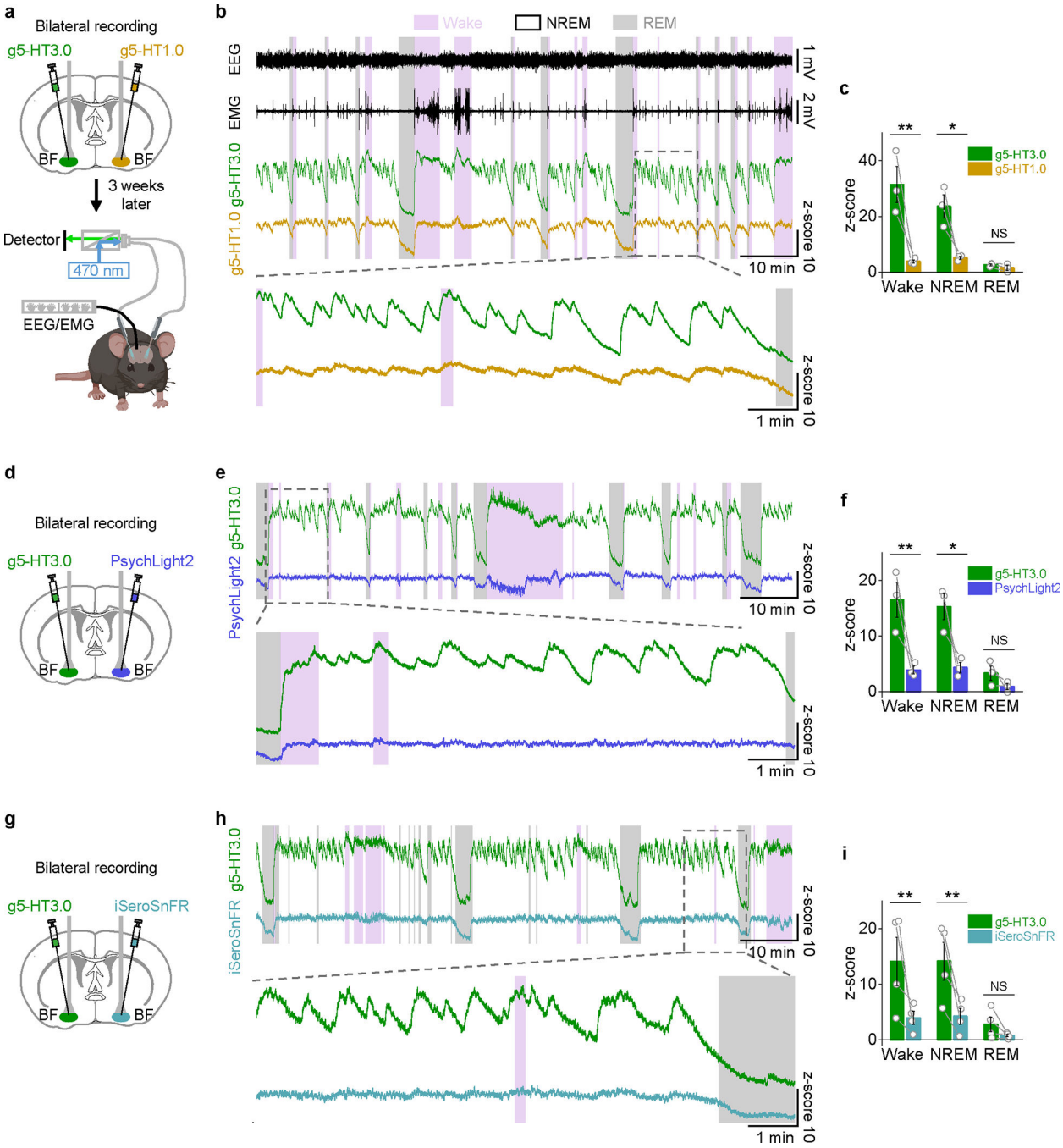

Extended Data Fig. 7 |. Comparison of gGRAB$_{5\text{-}HT3.0}$ and other green 5-HT sensors during the sleep-wake cycle in freely moving mice.

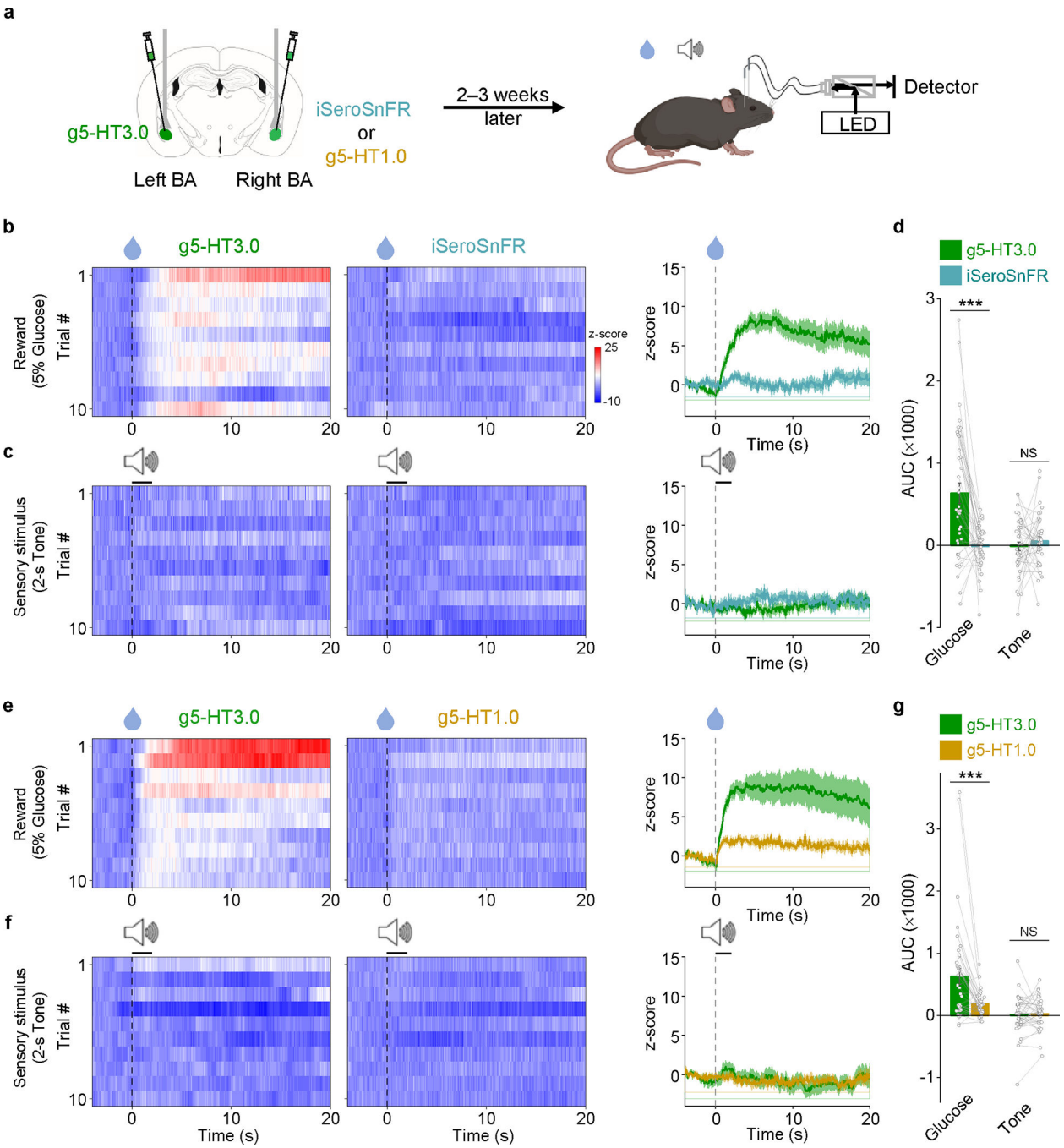

Extended Data Fig. 8 |. Comparison of gGRAB$_{5\text{-}HT3.0}$ and other green 5-HT sensors during reward and tone delivery.

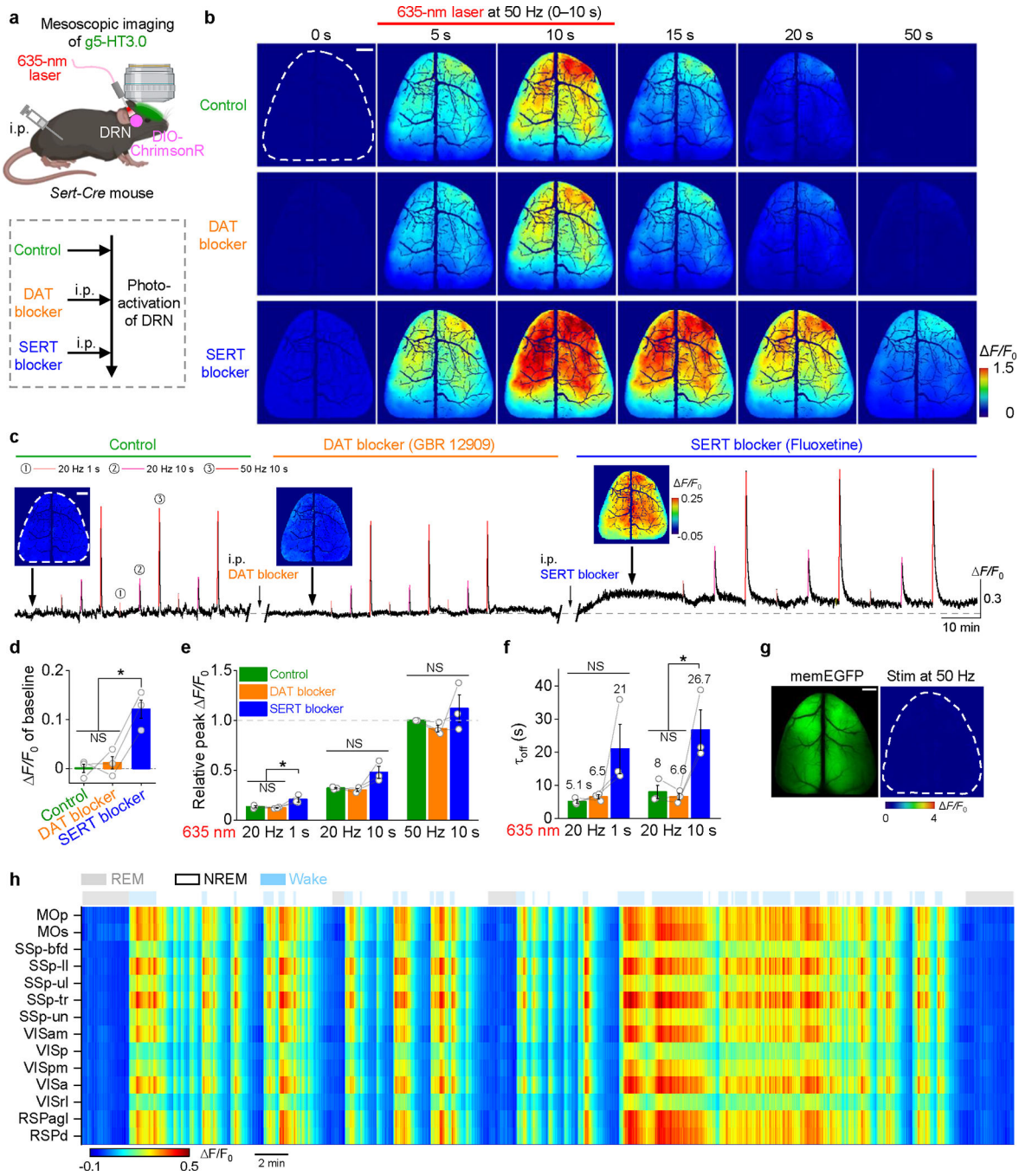

Extended Data Fig. 9 |. gGRAB$_{5\text{-}HT3.0}$ reveals 5-HT dynamics in mouse dorsal cortex *in vivo*.

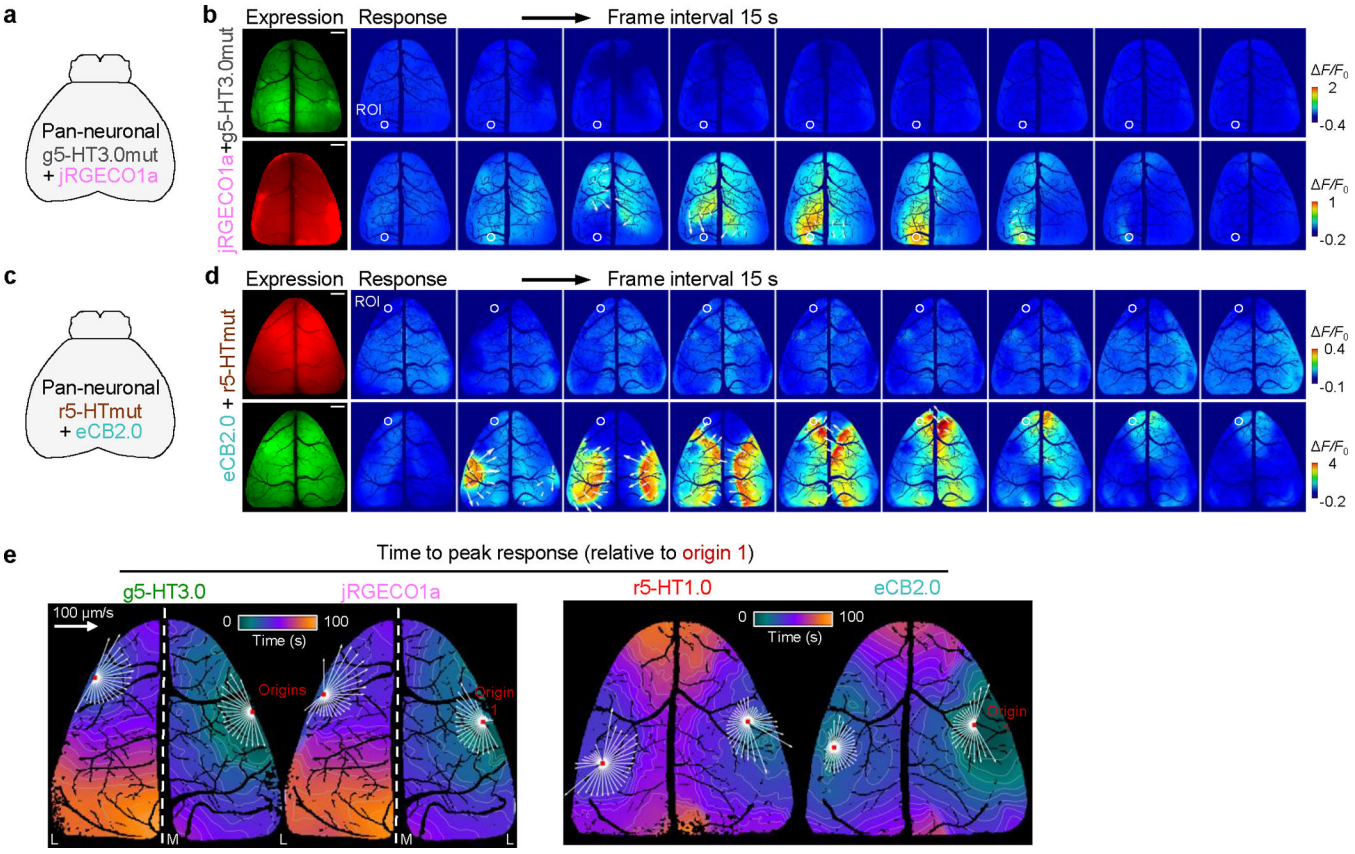

Extended Data Fig. 10 |. Mesoscopic imaging of 5-HT, Ca^{2+} and eCB waves during seizures.

Supplementary Material

Refer to Web version on PubMed Central for supplementary material.

Acknowledgments

This work was supported by the National Key R&D Program of China (2022YFC3300905 to H.D.); the National Key R&D Program of China (2022YFE0108700), the National Natural Science Foundation of China (31925017), the Beijing Municipal Science & Technology Commission (Z220009), the NIH BRAIN Initiative (1U01NS113358 and 1U01NS120824), grants from the Peking-Tsinghua Center for Life Sciences and the State Key Laboratory of Membrane Biology at Peking University School of Life Sciences, the Feng Foundation of Biomedical Research, the Clement and Xinxin Foundation, and the New Cornerstone Science Foundation through the New Cornerstone Investigator Program and the XPLORER PRIZE (to Y.L.); the National Major Project of China Science and Technology Innovation 2030 for Brain Science and Brain-Inspired Technology (2022ZD0205600), the Postdoctoral Science Foundation (2022M720258), the Peking University Boya Postdoctoral Fellowship (to J.W.); Key Laboratory of Drug Monitoring and Control, Drug Intelligence and Forensic Center, Ministry of Public Security, P.R. (2022-KLDMC-03 to H.D.). We thank Y. Rao at Peking University for providing the LSM710 confocal microscope and sharing *Sert-Cre* mice, X. Lei at PKU-CLS for providing the Opera Phenix high-content screening system, and the National Center for Protein Sciences at Peking University in Beijing, China, for support and assistance with the imaging platform and behavioral experiments. We thank P. Gong at the University of Sydney and M. Mohajerani at University of Lethbridge for their help with the optical flow analysis of waves. Components in cartoon illustrations, including Figs. 3a, 3f, 4a, 5a, Extended Data Figs. 4c (right), 4d–f (left), 7a, 8a, 9a and Supplementary Fig. 2a, were created with BioRender.com.

Data availability

The plasmids used to express the sensors in this study and the related sequences are available from Addgene (catalog nos. 208709–208727; https://www.addgene.org/Yulong_Li/). The human GPCR cDNA library was obtained from the hORFeome database 8.1 (http://horfdb.dfci.harvard.edu/index.php?page=home). Source data are provided with this paper.

References

1. Berger M, Gray JA & Roth BL The expanded biology of serotonin. Annu. Rev. Med. 60, 355–366 (2009). [PubMed: 19630576]
2. Li Y et al. Serotonin neurons in the dorsal raphe nucleus encode reward signals. Nat Commun. 7, 10503 (2016). [PubMed: 26818705]
3. Portas CM et al. On-line detection of extracellular levels of serotonin in dorsal raphe nucleus and frontal cortex over the sleep/wake cycle in the freely moving rat. Neuroscience 83, 807–814 (1998). [PubMed: 9483564]
4. Lesch KP et al. Association of anxiety-related traits with a polymorphism in the serotonin transporter gene regulatory region. Science 274, 1527–1531 (1996). [PubMed: 8929413]
5. Theodore WH, Juhasz C, Savic V & Drevets W Serotonin, depression, and epilepsy. Epilepsia 46, 3–3 (2005).
6. Li Y et al. Synaptic mechanism underlying serotonin modulation of transition to cocaine addiction. Science 373, 1252–1256 (2021). [PubMed: 34516792]
7. Vaswani M, Linda FK & Ramesh S Role of selective serotonin reuptake inhibitors in psychiatric disorders: a comprehensive review. Prog. Neuropsychopharmacol. Biol. Psychiatry 27, 85–102 (2003). [PubMed: 12551730]
8. Fuller RW Uptake inhibitors increase extracellular serotonin concentration measured by brain microdialysis. Life Sci. 55, 163–167 (1994). [PubMed: 8007758]
9. Lama RD, Charlson K, Anantharam A & Hashemi P Ultrafast detection and quantification of brain signaling molecules with carbon fiber microelectrodes. Anal. Chem. 84, 8096–8101 (2012). [PubMed: 22881278]
10. Candelario J & Chachisvilis M Mechanical stress stimulates conformational changes in 5-hydroxytryptamine receptor 1B in bone cells. Cell. Mol. Bioeng. 5, 277–286 (2012).
11. Wan J et al. A genetically encoded sensor for measuring serotonin dynamics. Nat. Neurosci. 24, 746–752 (2021). [PubMed: 33821000]
12. Dong C et al. Psychedelic-inspired drug discovery using an engineered biosensor. Cell 184, 2779–2792.e2718 (2021). [PubMed: 33915107]
13. Kubitschke M et al. Next generation genetically encoded fluorescent sensors for serotonin. Nat. Commun. 13, 7525 (2022). [PubMed: 36473867]
14. Unger EK et al. Directed evolution of a selective and sensitive serotonin sensor via machine learning. Cell 183, 1986–2002.e1926 (2020). [PubMed: 33333022]
15. Guiard BP, El Mansari M, Merali Z & Blier P Functional interactions between dopamine, serotonin and norepinephrine neurons: an in-vivo electrophysiological study in rats with monoaminergic lesions. Int. J. Neuropsychopharmacol. 11, 625–639 (2008). [PubMed: 18205979]
16. Jeong S et al. High-throughput evolution of near-infrared serotonin nanosensors. Science Advances 5, eaay3771 (2019). [PubMed: 31897432]
17. Dana H et al. Sensitive red protein calcium indicators for imaging neural activity. eLife 5, e12727 (2016). [PubMed: 27011354]
18. Feng J et al. A genetically encoded fluorescent sensor for rapid and specific in vivo detection of norepinephrine. Neuron 102, 745–761.e748 (2019). [PubMed: 30922875]
19. Sun F et al. Next-generation GRAB sensors for monitoring dopaminergic activity in vivo. Nat. Methods 17, 1156–1166 (2020). [PubMed: 33087905]

20. Bajar BT et al. Improving brightness and photostability of green and red fluorescent proteins for live cell imaging and FRET reporting. Sci. Rep. 6, 20889 (2016). [PubMed: 26879144]
21. Pédelacq J-D, Cabantous S, Tran T, Terwilliger TC & Waldo GS Engineering and characterization of a superfolder green fluorescent protein. Nat. Biotechnol. 24, 79–88 (2006). [PubMed: 16369541]
22. Peng Y et al. 5-HT2C receptor structures reveal the structural basis of GPCR polypharmacology. Cell 172, 719–730.e714 (2018). [PubMed: 29398112]
23. Ballesteros JA & Weinstein H in Methods in Neurosciences, Vol. 25. (ed. Sealfon SC) 366–428 (Academic Press, 1995).
24. Wan Q et al. Mini G protein probes for active G protein-coupled receptors (GPCRs) in live cells. J. Biol. Chem. 293, 7466–7473 (2018). [PubMed: 29523687]
25. Kroeze WK et al. PRESTO-Tango as an open-source resource for interrogation of the druggable human GPCRome. Nat. Struct. Mol. Biol. 22, 362–369 (2015). [PubMed: 25895059]
26. Zhuo Y et al. Improved green and red GRAB sensors for monitoring dopaminergic activity in vivo. Nat. Methods (2023).
27. Nagel G et al. Channelrhodopsin-2, a directly light-gated cation-selective membrane channel. Proc. Natl. Acad. Sci. USA 100, 13940–13945 (2003). [PubMed: 14615590]
28. Zhuang X, Masson J, Gingrich JA, Rayport S & Hen R Targeted gene expression in dopamine and serotonin neurons of the mouse brain. Journal of Neuroscience Methods 143, 27–32 (2005). [PubMed: 15763133]
29. Broussard GJ et al. In vivo measurement of afferent activity with axon-specific calcium imaging. Nat. Neurosci. 21, 1272–1280 (2018). [PubMed: 30127424]
30. Xu M et al. Basal forebrain circuit for sleep-wake control. Nat. Neurosci. 18, 1641–1647 (2015). [PubMed: 26457552]
31. Oh SW et al. A mesoscale connectome of the mouse brain. Nature 508, 207–214 (2014). [PubMed: 24695228]
32. Hamodi AS, Sabino AM, Fitzgerald ND, Moschou D & Crair MC Transverse sinus injections drive robust whole-brain expression of transgenes. eLife 9 (2020).
33. Ferezou I et al. Spatiotemporal dynamics of cortical sensorimotor integration in behaving mice. Neuron 56, 907–923 (2007). [PubMed: 18054865]
34. Klapoetke NC et al. Independent optical excitation of distinct neural populations. Nat. Methods 11, 338–346 (2014). [PubMed: 24509633]
35. Wang QX et al. The allen mouse brain common coordinate framework: a 3D reference atlas. Cell 181, 936–953.e920 (2020). [PubMed: 32386544]
36. Pasini A, Tortorella A & Gale K The anticonvulsant action of fluoxetine in substantia nigra is dependent upon endogenous serotonin. Brain Res. 724, 84–88 (1996). [PubMed: 8816259]
37. Tecott LH et al. Eating disorder and epilepsy in mice lacking 5-HT2C serotonin receptors. Nature 374, 542–546 (1995). [PubMed: 7700379]
38. Cheng H-M, Gao C-S, Lou Q-W, Chen Z & Wang Y The diverse role of the raphe 5-HTergic systems in epilepsy. Acta Pharmacol. Sin. 43, 2777–2788 (2022). [PubMed: 35614227]
39. Lin W. h. et al. Seizure-induced 5-HT release and chronic impairment of serotonergic function in rats. Neurosci. Lett. 534, 1–6 (2013). [PubMed: 23276638]
40. Dong A et al. A fluorescent sensor for spatiotemporally resolved imaging of endocannabinoid dynamics in vivo. Nat. Biotechnol, 787–798 (2021).
41. Ben-Ari Y, Lagowska J, Tremblay E & Le Gal La Salle G. A new model of focal status epilepticus: intra-amygdaloid application of kainic acid elicits repetitive secondarily generalized convulsive seizures. Brain Res. 163, 176–179 (1979). [PubMed: 427540]
42. Farrell JS et al. In vivo assessment of mechanisms underlying the neurovascular basis of postictal amnesia. Sci. Rep. 10 (2020).
43. Bunin MA & Wightman RM Quantitative evaluation of 5-hydroxytryptamine (serotonin) neuronal release and uptake: An investigation of extrasynaptic transmission. J. Neurosci. 18, 4854–4860 (1998). [PubMed: 9634551]

44. Thorré K et al. Differential effects of restraint stress on hippocampal 5-HT metabolism and extracellular levels of 5-HT in streptozotocin-diabetic rats. Brain Res. 772, 209–216 (1997). [PubMed: 9406974]
45. Hashemi P, Dankoski EC, Petrovic J, Keithley RB & Wightman RM Voltammetric detection of 5-hydroxytryptamine release in the rat brain. Anal. Chem. 81, 9462–9471 (2009). [PubMed: 19827792]
46. Subach OM et al. Conversion of red fluorescent protein into a bright blue probe. Chem. Biol. 15, 1116–1124 (2008). [PubMed: 18940671]
47. Shen H-W et al. Regional differences in extracellular dopamine and serotonin assessed by in vivo microdialysis in mice lacking dopamine and/or serotonin transporters. Neuropsychopharmacology 29, 1790–1799 (2004). [PubMed: 15226739]
48. Gibson DG et al. Enzymatic assembly of DNA molecules up to several hundred kilobases. Nat. Methods 6, 343–345 (2009). [PubMed: 19363495]
49. Yusa K, Zhou L, Li MA, Bradley A & Craig NL A hyperactive piggyBac transposase for mammalian applications. Proc. Natl. Acad. Sci. USA 108, 1531–1536 (2011). [PubMed: 21205896]
50. Wang Y et al. Accurate quantification of astrocyte and neurotransmitter fluorescence dynamics for single-cell and population-level physiology. Nat. Neurosci. 22, 1936–1944 (2019). [PubMed: 31570865]
51. Barger Z, Frye CG, Liu DQ, Dan Y & Bouchard KE Robust, automated sleep scoring by a compact neural network with distributional shift correction. PLoS One 14 (2019).
52. Werley CA, Chien MP & Cohen AE Ultrawidefield microscope for high-speed fluorescence imaging and targeted optogenetic stimulation. Biomedical Optics Express 8, 5794–5813 (2017). [PubMed: 29296505]
53. Zhuang C et al. Real-time brain-wide multi-planar microscopy for simultaneous cortex and hippocampus imaging at the cellular resolution in mice. Biomedical Optics Express 12, 1858–1868 (2021). [PubMed: 33996203]
54. Jackson J, Karnani MM, Zemelman BV, Burdakov D & Lee AK Inhibitory control of prefrontal cortex by the claustrum. Neuron 99, 1029–1039.e1024 (2018). [PubMed: 30122374]
55. Pnevmatikakis EA & Giovannucci A NoRMCorre: An online algorithm for piecewise rigid motion correction of calcium imaging data. J. Neurosci. Methods 291, 83–94 (2017). [PubMed: 28782629]
56. Arganda-Carreras I et al. Trainable Weka Segmentation: a machine learning tool for microscopy pixel classification. Bioinformatics 33, 2424–2426 (2017). [PubMed: 28369169]
57. Zimmermann T Spectral imaging and linear unmixing in light microscopy. Adv. Biochem. Eng. Biotechnol. 95, 245–265 (2005). [PubMed: 16080271]
58. Ma Y et al. Wide-field optical mapping of neural activity and brain haemodynamics: considerations and novel approaches. Philosophical Transactions of the Royal Society B: Biological Sciences 371, 20150360 (2016).
59. Valley MT et al. Separation of hemodynamic signals from GCaMP fluorescence measured with wide-field imaging. J. Neurophysiol. 123, 356–366 (2020). [PubMed: 31747332]
60. Vesuna S et al. Deep posteromedial cortical rhythm in dissociation. Nature 586, 87–94 (2020). [PubMed: 32939091]
61. Musall S, Kaufman MT, Juavinett AL, Gluf S & Churchland AK Single-trial neural dynamics are dominated by richly varied movements. Nat. Neurosci. 22, 1677–1686 (2019). [PubMed: 31551604]
62. Saxena S et al. Localized semi-nonnegative matrix factorization (LocaNMF) of widefield calcium imaging data. PLoS Comp. Biol. 16, e1007791 (2020).
63. Townsend RG & Gong P Detection and analysis of spatiotemporal patterns in brain activity. PLoS Comp. Biol. 14, e1006643 (2018).

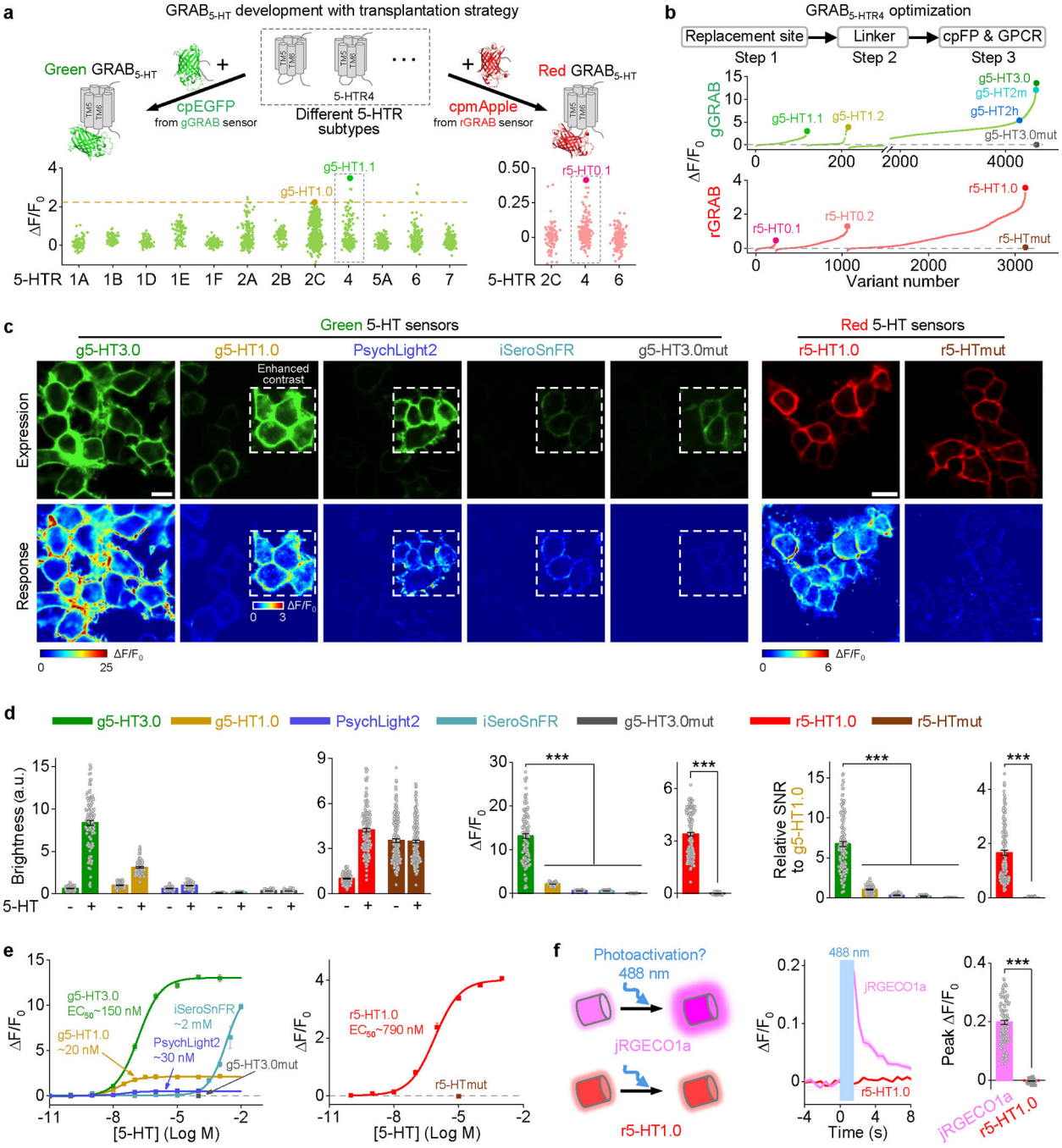

Fig. 1 |. Development of improved green fluorescent 5-HT sensors and red 5-HT sensors.

a, Schematic illustrating the strategy for developing $GRAB_{5\text{-}HT}$ sensors (top). Performance of sensor candidates based on different receptor subtypes for green (bottom left) and red 5-HT sensors (bottom right). The dashed horizontal line represents g5-HT1.0 response (bottom left), and the best candidates in green and red sensors are denoted by enlarged green and pink dots, respectively.

b, Optimization of the replacement site, linker, cpFP and GPCR. Responses to 10 μM 5-HT of various candidates are presented, and different versions are indicated with enlarged dots.

c, Representative images of sensors' expression (top, with 5-HT) and response (bottom) to 5-HT in HEK293T cells. Insets with white dashed outlines in images have either enhanced contrast (top) or different pseudocolor scales (bottom). 100 μM 5-HT for green sensors and 10 μM 5-HT for red sensors. Similar results were observed for more than 50 cells. Scale bar, 20 μm.

d, Group summary of the brightness (left), peak $\Delta F/F_0$ (middle) and SNR (right) of different 5-HT sensors. The SNR of all sensors were relative to g5-HT1.0; a.u., arbitrary units, the basal brightness of g5-HT1.0 is set as 1. $n = 119$ cells from 3 coverslips (hereafter denoted as 119/3) for g5-HT3.0, 82/3 for g5-HT1.0, 64/3 for PsychLight2, 139/3 for iSeroSnFR, 92/3 for g5-H3.0mut, 159/5 for r5-HT1.0 and 191/5 for r5-HTmut; 100 μM 5-HT for green sensors and 10 μM 5-HT for red sensors. (One-way ANOVA followed by Tukey's multiple-comparison tests for green sensors; for peak $\Delta F/F_0$, $F_{4,491} = 387.1$, $P = 2.76 \times 10^{-150}$, post hoc test: $P = 0$, 4.15×10^{-9}, 0 and 0 for g5-HT3.0 versus other sensors; for relative SNR, $F_{4,491} = 285.7$, $P = 1.13 \times 10^{-126}$, post hoc test: $P = 5.62 \times 10^{-7}$, 2.22×10^{-8}, 7.33×10^{-8} and 4×10^{-9} for g5-HT3.0 versus other sensors. Two-tailed Student's *t*-test for r5-HT1.0 and r5-HTmut; for peak $\Delta F/F_0$, $P = 3.13 \times 10^{-72}$; for relative SNR, $P = 2.67 \times 10^{-43}$.)

e, Dose-response curves of different 5-HT sensors. $n = 3$ wells for each sensor with 300–500 cells per well.

f, Schematic illustrates the photoactivation properties of jRGECO1a and r5-HT1.0 (left), representative traces (middle) and group summary of peak $\Delta F/F_0$ (right) in response to blue light (488 nm, without imaging) in cells expressing jRGECO1a or r5-HT1.0. $n = 105/4$ for jRGECO1a and 88/4 for r5-HT1.0. (Two-tailed Student's *t*-test, $P = 2.07 \times 10^{-48}$).

Data are shown as mean ± SEM in **d–f**, with the error bars or shaded regions indicating the SEM, $^{***}P < 0.001$.

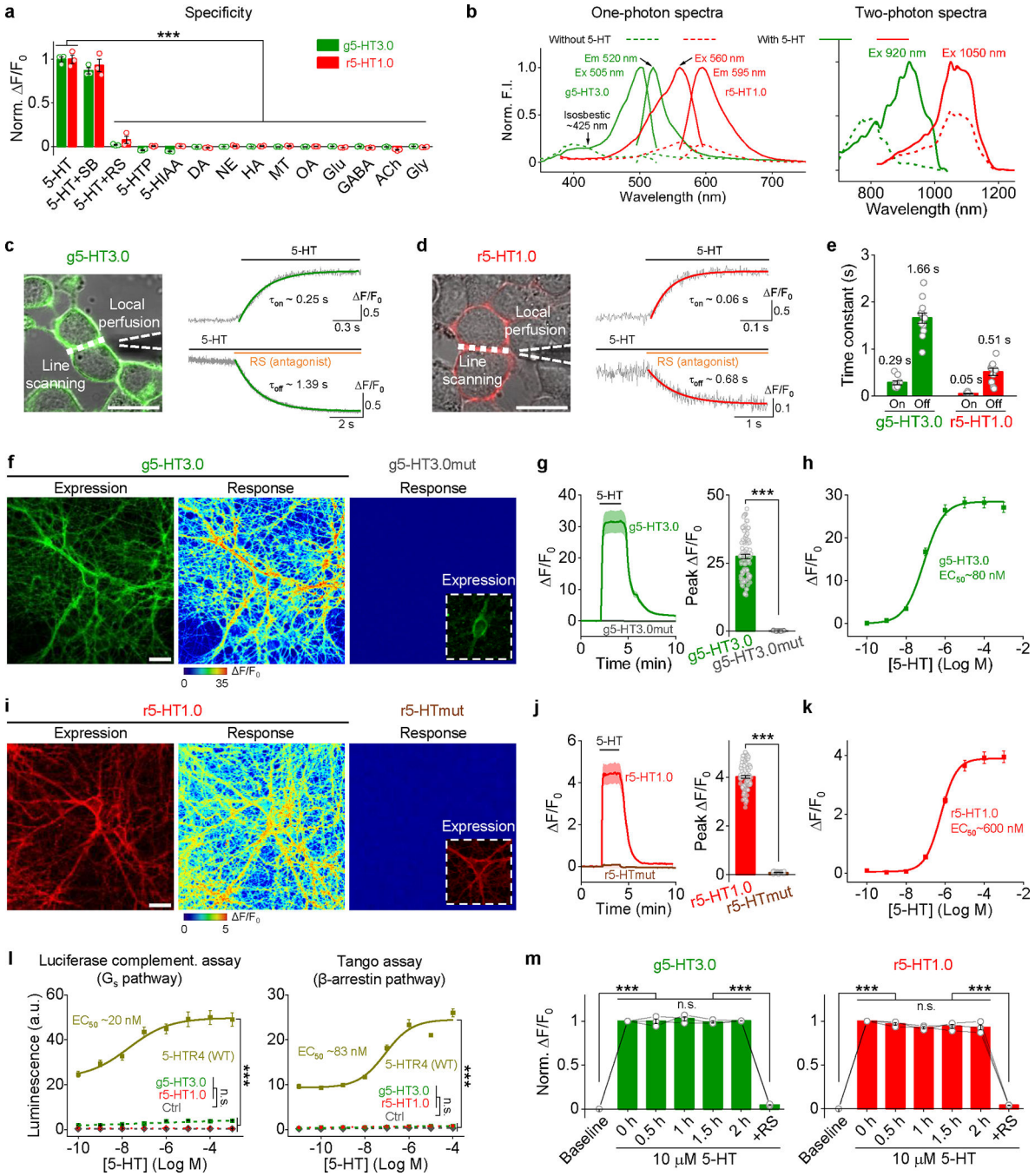

Fig. 2 |. Characterization of 5-HT sensors in HEK293T cells and cultured rat cortical neurons.

a, Normalized $\Delta F/F_0$ of g5-HT3.0 and r5-HT1.0 in response to different compounds (each at 10 μM except RS at 100 μM). 5-HTP, 5-hydroxytryptophan; 5-HIAA, 5-hydroxyindole acetic acid; DA, dopamine; NE, norepinephrine; HA, histamine; MT, melatonin; OA, octopamine; Glu, glutamate; GABA, gamma-aminobutyric acid; ACh, acetylcholine; Gly, glycine. Norm., normalized. $n = 3$ wells per group, 200–500 cells per well. (One-way ANOVA followed by Tukey's multiple-comparison tests, for g5-HT3.0, $F_{13,28} = 745.7$, $P = 5.74 \times 10^{-32}$, post hoc test: $P = 0$ for 5-HT versus 5-HT and RS, and other compounds; for

r5-HT1.0, $F_{13,28}$ = 180.6, P = 2.02 × 10^{-23}, post hoc test: P = 0 for 5-HT versus 5-HT and RS, and other compounds.)

b, One-photon excitation (Ex) and emission (Em) spectra and two-photon excitation spectra of g5-HT3.0 and r5-HT1.0 in the absence (dashed line) and presence of 10 μM 5-HT (solid line). F.I., fluorescence intensity.

c–e, Kinetic of g5-HT3.0 and r5-HT1.0 in cultured HEK293T cells. Illustration of the local puffing system (**c,d**, left). Representative traces of sensor fluorescence increase to 5-HT puffing (**c,d**, top right) and decrease to RS puffing (**c,d**, bottom right). Group summary of on and off kinetics (**e**). n = 10 cells from 3 coverslips (short for 10/3) for g5-HT3.0 on kinetics, 12/4 for g5-HT3.0 off kinetics, 9/3 for r5-HT1.0 on kinetics, 12/4 for r5-HT1.0 off kinetics.

f, Representative images showing the expression and responses of g5-HT3.0 and g5-HT3.0mut to 100 μM 5-HT in cultured rat cortical neurons. The inset in the g5-HT3.0mut response image shows the contrast-enhanced expression image.

g, Representative traces and peak response summary of g5-HT3.0 and g5-HT3.0mut in response to 100 μM 5-HT. n = 96 regions of interest (ROIs) from 5 coverslips (short for 96/5) for g5-HT3.0 and 92/5 for g5-HT3.0mut. (Two-tailed Student's t-test, P = 1.40 × 10^{-53} for g5-HT3.0 versus g5-HT3.0mut.)

h, The dose-response curve of g5-HT3.0. n = 76/4.

i, Representative images showing the expression and responses of r5-HT1.0 and r5-HTmut to 10 μM 5-HT.

j, Representative traces and peak response summary of r5-HT1.0 and r5-HTmut in response to 10 μM 5-HT. n = 80/4 for r5-HT1.0 and 60/3 for r5-HTmut. (Two-tailed Student's t-test, P = 4.46 × 10^{-70} for r5-HT1.0 versus r5-HTmut.)

k, The dose-response curve of r5-HT1.0. n = 80/4.

l, Downstream coupling tests. WT, wild type; Ctrl, control, without expression of wild type 5-HTR4 or sensors; a.u., arbitrary units. n = 3 wells per group, 200–500 cells per well. (One-way ANOVA followed by Tukey's multiple-comparison tests, for luciferase complementation assay, $F_{3,8}$ = 256, P = 2.77 × 10^{-8}, post hoc test: P = 0 and 0.37 for g5-HT3.0 versus 5-HTR4 (WT) and Ctrl in 1 mM 5-HT, respectively, P = 0 and 1 for r5-HT1.0 versus 5-HTR4 (WT) and Ctrl, respectively; for Tango assay, $F_{3,8}$ = 766.4, P = 3.55 × 10^{-10}, post hoc test: P = 0 and 0.89 for g5-HT3.0 versus 5-HTR4 (WT) and Ctrl in 100 μM 5-HT, respectively, P = 0 and 0.86 for r5-HT1.0 versus 5-HTR4 (WT) and Ctrl, respectively.)

m, Normalized $\Delta F/F_0$ of g5-HT3.0 and r5-HT1.0 in response to the 2-h application of 10 μM 5-HT, followed by 100 μM RS. n = 3 wells for each sensor. (One-way repeated measures ANOVA followed by Tukey's multiple-comparison tests, for g5-HT3.0, F = 359.8, P = 0.034, post hoc test: P = 1.29 × 10^{-6} for baseline versus 0 h, P = 1.76 × 10^{-6} for 2.0 h versus RS, P = 1, 0.77, 1, 1 for 0 h versus 0.5 h, 1 h, 1.5 h or 2.0 h, respectively; for r5-HT1.0, F = 250.9, P = 0.04, post hoc test: P = 2.85 × 10^{-6} for baseline versus 0 h, P = 5.82 × 10^{-6} for 2.0 h versus RS, P = 0.95, 0.44, 0.66, 0.64 for 0 h versus 0.5 h, 1 h, 1.5 h or 2.0 h, respectively.)

a–e and **l** tested in HEK293T cells; **f–k** and **m** tested in cultured rat cortical neurons.

All scale bar, 20 μm. Data are shown as mean ± SEM in **a,e,g,h,j–m**, with the error bars or shaded regions indicating the SEM. ***P < 0.001, n.s., not significant.

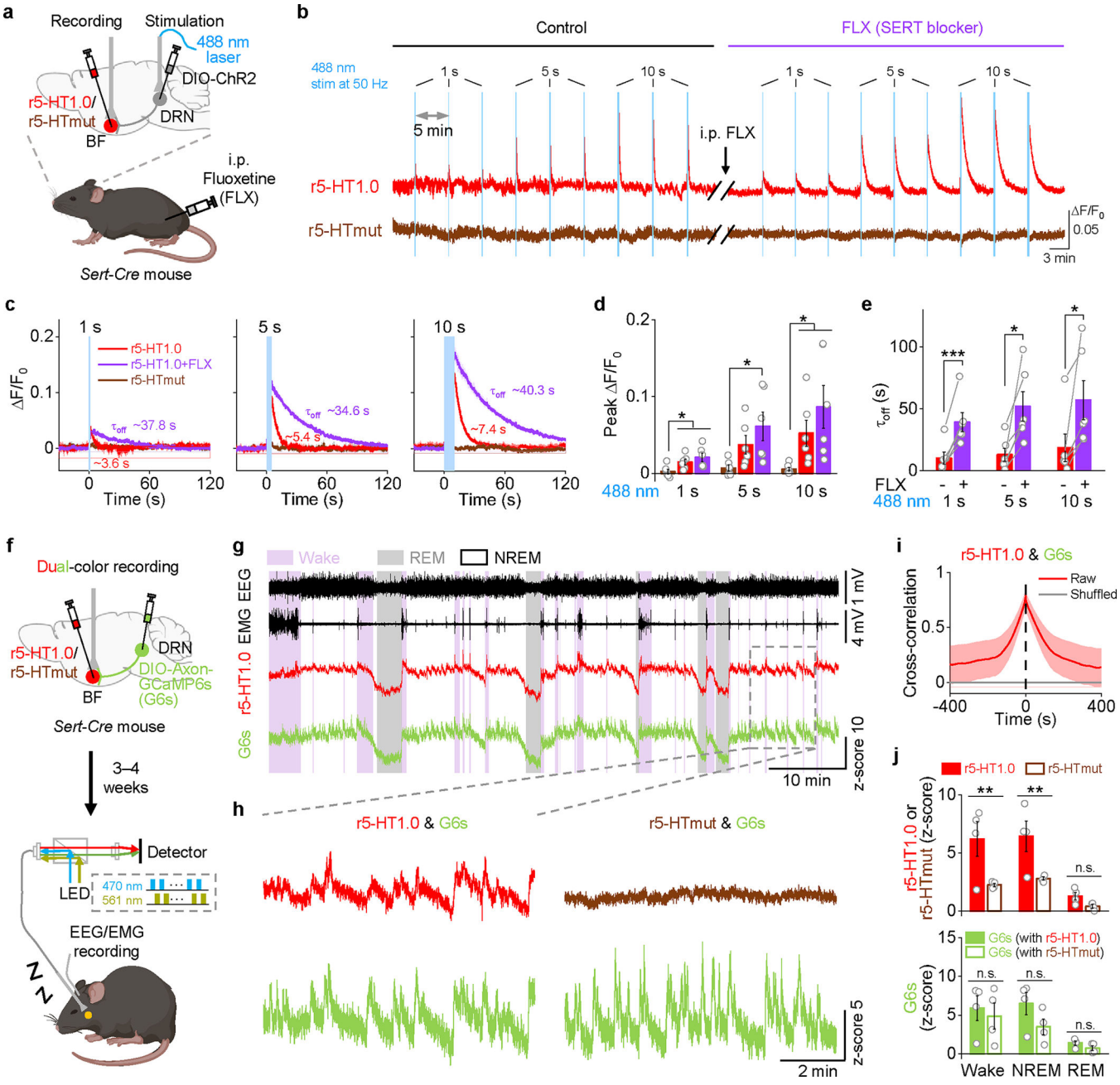

Fig. 3 |. Red GRAB$_{5\text{-HT}}$ sensor can monitor endogenous 5-HT release in freely moving mice.

a, Schematic depicting the fiber-photometry recording setup using red 5-HT sensors with optogenetic activation of DRN in *Sert-Cre* mice.

b, Representative $\Delta F/F_0$ traces of r5-HT1.0 and r5-HTmut in response to optical stimulation in the DRN under different stimulation durations before or after fluoxetine (FLX) application. Blue shading, period for 488-nm stimulation.

c, Average $\Delta F/F_0$ traces of r5-HT1.0 and r5-HTmut under different stimulation durations in an example mouse.

d, Summarized peak responses of r5-HT1.0 and r5-HTmut under different stimulation durations. $n = 6$ mice for each treatment. (Two-tailed Student's *t*-tests, for r5-HTmut versus r5-HT1.0, $P = 0.030$, 0.052, 0.041 under 1 s, 5 s, 10 s stimulation, respectively; for r5-HTmut versus r5-HT1.0+FLX, $P = 0.016$, 0.034, 0.033 under 1 s, 5 s, 10 s stimulation, respectively.)

e, Summarized decay kinetics of r5-HT1.0 with or without FLX application under different stimulation durations. $n = 6$ mice for each treatment. (Two-tailed paired *t*-tests for r5-HT1.0 and r5-HT1.0 + FLX, $P = 4.44 \times 10^{-4}$, 1.44×10^{-2}, 3.19×10^{-2} for 1 s, 5 s and 10 s stimulation, respectively.)

f, Schematic showing the setup for dual-color recording of r5-HT1.0 or r5-HTmut and GCaMP6s (G6s) during sleep-wake cycles.

g, Representative traces of simultaneous EEG, EMG, r5-HT1.0, and G6s recording during sleep-wake cycles in freely behaving mice. Pink shading, wake state; gray shading, REM sleep.

h, Zoom-in traces of r5-HT1.0 and G6s (from g) or r5-HTmut and G6s (mainly during the NREM sleep).

i, The average cross-correlation between r5-HT1.0 and G6s signals during sleep-wake cycles.

j, Average responses of 5-HT sensors (red channel, r5-HT1.0 or r5-HTmut) and G6s (green channel). $n = 4$ mice for each group. (Two-way repeated measures ANOVA followed by Tukey's multiple-comparison tests; for r5-HT1.0 versus r5-HTmut, post hoc test: $P = 5.65 \times 10^{-3}$, 9.22×10^{-3} and 0.47 during wake, NREM and REM sleep state, respectively; for G6s (with r5-HT1.0) versus G6s (with r5-HTmut), post hoc test: $P = 0.56$, 0.11 and 0.71 during wake, NREM and REM sleep state, respectively.)

Data are shown as mean ± SEM in **c–e,i,j**, with the error bars or shaded regions indicating the SEM, $*P < 0.05$, $**P < 0.01$, $***P < 0.001$, n.s., not significant.

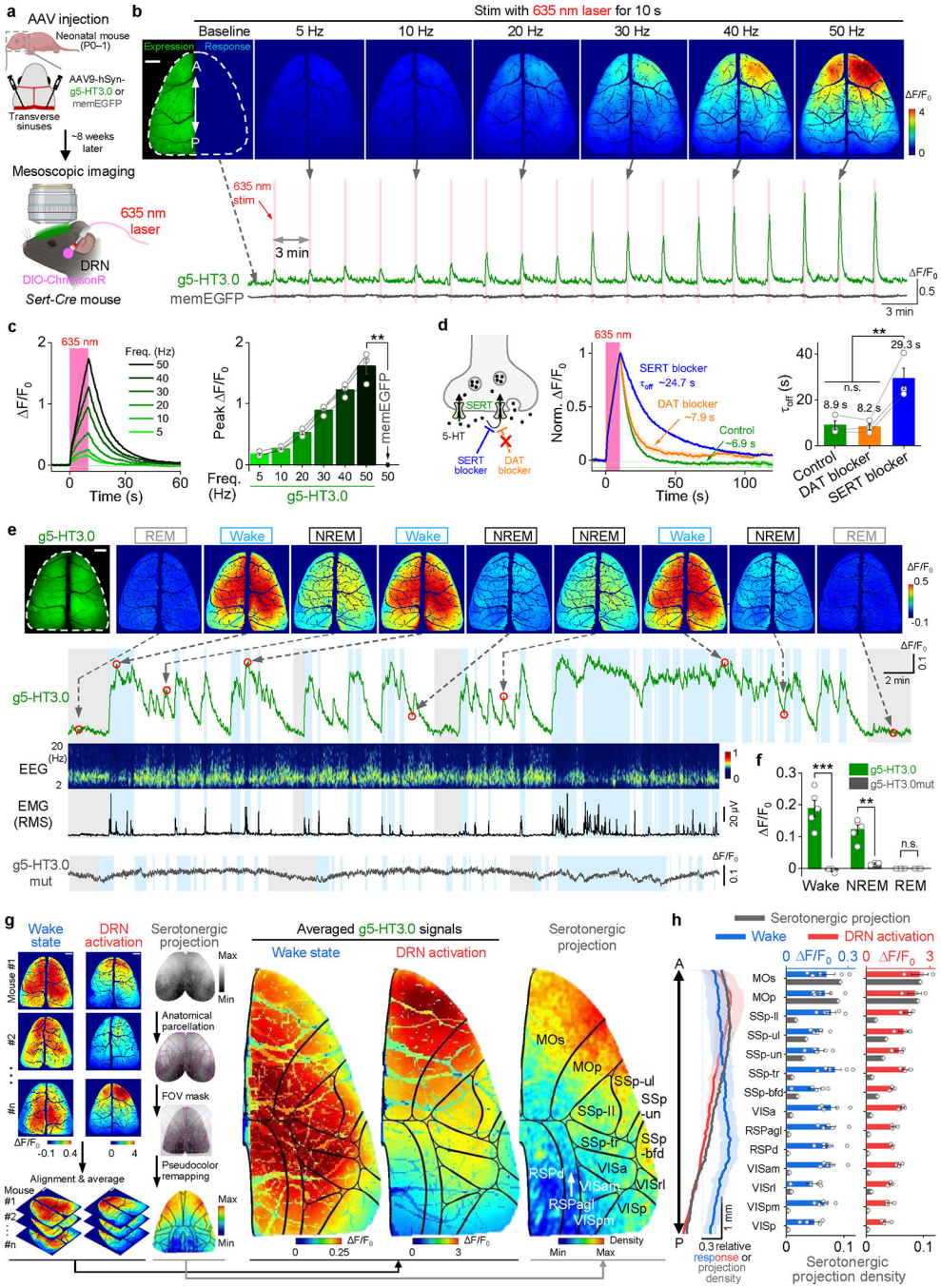

Fig. 4 |. gGRAB$_{5\text{-}HT3.0}$ reveals 5-HT release in mouse dorsal cortex *in vivo* by mesoscopic imaging.

a, Schematic depicting the mesoscopic imaging experiments.

b, Representative images showing the cortical g5-HT3.0 expression and response to optical stimulation in the DRN with incremental frequencies (top). Representative traces of g5-HT3.0 and a negative control memEGFP (bottom). The dashed white outline indicates the ROI.

c, Representative $\Delta F/F_0$ traces of g5-HT3.0 (left) and group data of peak response (right) with increased frequencies of 635 nm laser. $n = 3$ mice for each group. (Two-tailed Student's *t*-tests, $P = 8.48 \times 10^{-3}$ for g5-HT3.0 versus memEGFP under 50 Hz stimulation.)

d, Schematic illustrating the effect of SERT blocker and DAT blocker on extracellular 5-HT level (left). Representative $\Delta F/F_0$ traces of g5-HT3.0 (middle) and summary data of decay kinetics (right) during 50 Hz 10 s stimulation after treatment with indicated compounds. (One-way repeated measures ANOVA followed by Tukey's multiple-comparison tests, $F = 28.9$, $P = 4.18 \times 10^{-3}$, post hoc test: $P = 0.98$ for DAT blocker versus control, 6.45×10^{-3} for SERT blocker versus control and 5.72×10^{-3} for SERT blocker versus DAT blocker.)

e, Representative fluorescence and pseudocolor images of g5-HT3.0 during sleep-wake cycles (top). Representative traces of g5-HT3.0 response, EEG, EMG (by root mean square, RMS) and g5-HT3.0mut response in the dorsal cortex during sleep-wake cycles (bottom). The dashed white outline in the top left image indicates the ROI. Dashed arrows and red circles indicate the timepoint of frames shown at the top. Gray shading, REM sleep; light blue shading, wake state.

f, Group data of g5-HT3.0 and g5-HT3.0mut responses in mice during the awake state, NREM and REM sleep. $n = 5$ mice for g5-HT3.0 and 3 mice for g5-HT3.0mut. (Two-way repeated measures ANOVA followed by Tukey's multiple-comparison tests for g5-HT3.0 and g5-HT3.0mut, $P = 5.77 \times 10^{-6}$, 1.89×10^{-3} and 1 during the wake, NREM and REM sleep state, respectively.)

g, Snapshots of g5-HT3.0 responses in different mice in the awake state and DRN activation, and serotonergic projection map modified from Allen Brain (left). Average pseudocolor images of g5-HT3.0 responses under indicated conditions (middle) and serotonergic projection map overlaid with black outlines aligned to the Allen Mouse Brain CCF (right). $n = 5$ and 3 mice for the awake state and DRN activation group, respectively.

h, Average relative responses of g5-HT3.0 and serotonergic projection density along the anterior-to-posterior (AP) axis (left) and summary of g5-HT3.0 signals or serotonergic projection density in different cortex regions. $n = 5$ and 3 mice for the awake state and DRN activation group, respectively.

All scale bar, 1 mm. Data are shown as mean ± SEM in **c,d,f,h**, with the error bars or shaded regions indicating the SEM, **P < 0.01, ***P < 0.001, n.s., not significant.

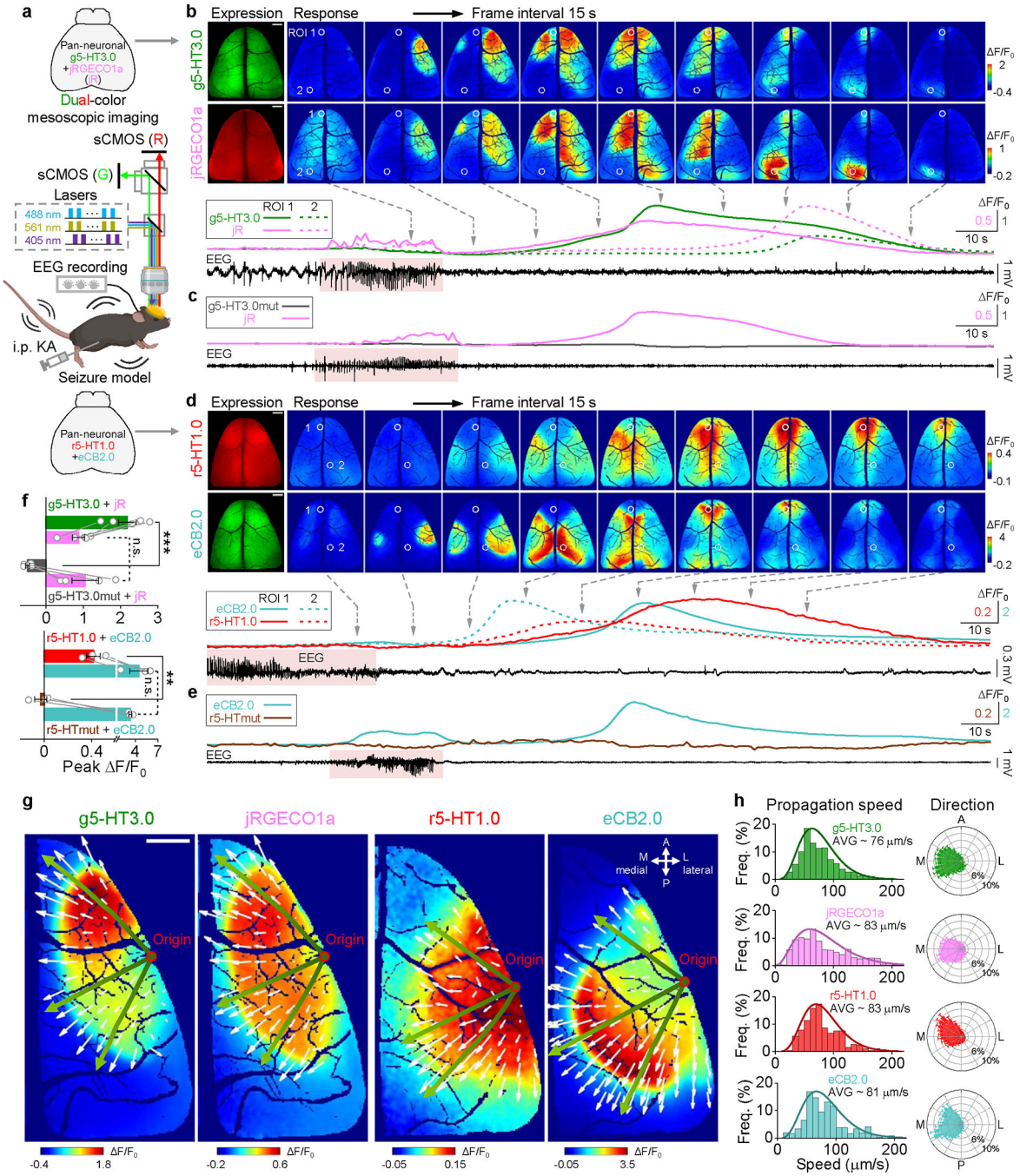

Fig. 5 |. Dual-color imaging of cortex-wide neurochemical waves during seizures.

a, Schematic depicting the setup of dual-color mesoscopic imaging in a KA-induced seizure model.

b, Representative images and $\Delta F/F_0$ traces of g5-HT3.0 and jRGECO1a during seizures. Two ROIs (500 μm in diameter) are labeled; ROI 1 (the white circle) and ROI 2 (the white dashed circle) show the maximum response regions of g5-HT3.0 and jRGECO1a, respectively. The solid and dashed lines in traces correspond to ROI 1 and ROI 2, respectively. The red shading in the EEG trace indicates the epileptic discharges.

c, Representative $\Delta F/F_0$ traces of g5-HT3.0mut and jRGECO1a during seizures, similar to b, and images are showed in Extended Data Fig. 9b.

d, Representative images and $\Delta F/F_0$ traces of r5-HT1.0 and eCB2.0 during seizures, similar to b, except that ROI 1 (the white circle) and ROI 2 (the white dashed circle) show the maximum response regions of r5-HT1.0 and eCB2.0, respectively.

e, Representative traces of r5-HTmut and eCB2.0 signals during seizures, similar to d, and images are showed in Extended Data Fig. 9d.

f, Group summary of different sensors' peak responses. $n = 5$ mice for the group co-expressing g5-HT3.0 and jRGECO1a, $n = 4$ for g5-HT3.0mut and jRGECO1a, $n = 3$ for r5-HT1.0 and eCB2.0, $n = 3$ for r5-HTmut and eCB2.0. (Two-tailed Student's *t*-tests, $P = 2.36 \times 10^{-4}$ for g5-HT3.0 versus g5-HT3.0mut, $P = 0.64$ for jRGECO1a between two groups; $P = 4.41 \times 10^{-3}$ for r5-HT1.0 versus r5-HTmut, $P = 0.45$ for eCB2.0 between two groups.)

g, Representative images showing the wave propagation detected by indicated sensors. The red circle indicates the origin of waves; small white arrows indicate the wave-propagating velocity vector; green lines with arrow indicate example propagating trajectories. L, lateral, M, medial, A, anterior, P, posterior.

h, Probability distributions of wave-propagating speed and direction calculated by indicated sensors.

Scale bar in all images, 1 mm. Data are shown as mean ± SEM in **f,h**, with the error bars indicating the SEM, $^{**}P < 0.01$, $^{***}P < 0.001$, n.s., not significant.